Bachelor thesis
BSc Applied Earth Sciences

Analysis and comparison of rock strength properties of calcarenite, acquired by needle penetration, unconfined compression and shear box tests

By C.B. Houkes

23 October 2013

Main supervisor: dr.ir. D.J.M. Ngan-Tillard, Geo-Engineering section
Second supervisor: dr. J.H.L. Voncken, Resource Engineering section

Department of Geoscience and Engineering
Faculty of Civil Engineering and Geosciences
Delft University of Technology, Delft, the Netherlands

Preface

By completing this Bachelor thesis, nearly two months of interesting but also rather intensive research, laboratory work and data processing has come to an end. I had the opportunity to learn various new skills regarding geotechnical laboratory work and also got a front-row insight into the construction of a cut-and-cover tunnel. I am very happy that I got the opportunity to do this research and I hope that the results presented in this report can be of advantage to geotechnical engineering decisions in the course of construction works for the new A2 tunnel, or in further research. I wish you a pleasant reading.

Delft, 23 October 2013

Acknowledgements

On this occasion I would like to thank everybody who supported me in completing this Bachelor research project: in the first place dr. D.J.M Ngan-Tillard, who gave me the unique opportunity to do this project under her supervision and who kindly advised and encouraged me throughout the research process.

Furthermore, I want to emphatically thank the lab technicians, A. Mulder and W. Verwaal, for their indispensable help and advice on setting up or operating laboratory equipment and during the analysis of the measurements. It was a very pleasant and educational experience working with you.

Finally, I would like to thank B. Vink and R. Servais from Avenue2 and/or Strukton, for arranging the access to and for guidance on the tunnel construction site and thereby making this research project possible in the first place.

Abstract

This study focuses on three different, often used methods to determine rock strength: needle penetration, unconfined compression and shear box tests. The investigations were done on calcarenite that was taken directly from the construction site of the new A2 highway tunnel in Maastricht, the Netherlands. Besides determining the strength, it was also intended to obtain a better understanding of the differences, advantages and disadvantages of each method with respect to the others. Additionally, empirical and theoretical relationships for estimating the unconfined compressive strength were evaluated.

Needle penetration tests gave questionable results, especially when trying to estimate the UCS by using an empirical relationship: estimations differed by a factor of 10 from actually measured UCS. Unconfined compression test results proved to be strongly affected by anisotropy due to sedimentary bedding, ranging from 0.12 MPa (parallel to bedding) to 0.45 MPa (perpendicular to bedding). Shear box tests yielded relatively high cohesions for this particular material, also depending strongly on the orientation of sedimentary bedding, ranging from 42 kPa (parallel) to 128 kPa (perpendicular). The estimation of UCS from cohesions and friction angles obtained by shear box tests, gave fair but not highly accurate approximations within ±25% of the actually measured UCS.

Table of contents

1 Introduction

The findings presented in this report are the result of a Bachelor (BSc) research project on the rock strength properties of calcarenite. Although in popular language the investigated material is more often called “mergel” (English: marl) by Dutchmen, the rock is basically carbonate sandstone with very high carbonate content and therefore should more properly be described as calcarenite [Maurenbrecher & Verwaal, 2007, and Berendsen, 2008].

This particular research project is part of a longer term and still ongoing site investigation programme for the construction of the new A2 highway tunnel through the city of Maastricht in the Netherlands. The investigated material is also taken from a freshly excavated part on the actual construction site in the Geusselt section of this new tunnel.

The purpose of this research is to find out the general rock strength properties by means of different testing methods and also to gain a better understanding of the differences, advantages and disadvantages of each method with respect to the others. Additionally, empirical and theoretical relationships for estimating the (unconfined compressive) strength are evaluated. Finally, the outcomes are compared with previously obtained strength data from nearby boreholes that are collected by P.M. Maurenbrecher and W. Verwaal since 2007.

1.1 Research question

In the course of this research, answers to the following research questions are tried to be found:

What is the real in situ strength of the calcarenite in which the A2 tunnel is being constructed?

Is the rock locally as weak as observed during site investigations carried out for the tender phase of the project, or were the cores damaged by rotary core drilling, causing the microstructure of the material to be destroyed and consequently the cohesion to be significantly reduced?

1.2 Methodology

From the tunnel construction site, large undisturbed block samples were taken for testing in the laboratory. The sampling location was chosen at close proximity to boreholes that were found to contain very weak calcarenite (see Appendix A).

From the large undisturbed calcarenite blocks, smaller subsamples were cut for further strength testing. Ideally, triaxial tests as during the preliminary borehole investigations should have been performed. But since the triaxial testing equipment was being refurbished, other strength tests were conducted, namely unconfined compression, shear box and needle penetration tests. Needle penetration tests are for approximate strength indication only. A more detailed explanation of materials and methods can be found chapter 3.

1.3 Impact on the construction project

Retaining structures for deep excavations are designed on the basis of certain strength parameters and can become very costly when very low strengths have to be taken into account, or when the uncertainties are high. A heavy observational programme has to be put in place to detect the response of the ground to construction works. Also, remedial measures in case of calamities are elaborated and ready to put in place if necessary.

Safety margins due to uncertainties and the heaviness of retaining structures due to low strength parameters can both be decreased, thus limiting total costs, when more detailed and less uncertain data on rock or soil strength would be available.

2 Background

This chapter provides some brief background information with regard to the geological setting and to the tunnel construction project itself, for a better conception of the general geological and geotechnical conditions under which the construction takes place.

2.1 Geological history and stratigraphy

During most of the geological history, the region that is nowadays known as the Netherlands was situated close to the equator (early Mesozoic) or even on the southern hemisphere (Palaeozoic). Its long-term situation on the edge of continental landmasses (first Avalonia, later Laurasia, Pangaea and finally Eurasia) and, moreover, the fact of not being part of any major orogeny, made the Netherlands the ideal place for sediments to accumulate. Hence the Dutch subsurface now consists of several kilometres of largely undisturbed sediments. Climatic conditions and relative sea level, however, changed a lot over time and therefore the sediment types vary widely from, inter alia, coal (Carboniferous) to shale and evaporites (Permian), and from sandstones (Triassic) to carbonates and shales again (Jurassic) [Berendsen, 2008].

During Cretaceous, when the continents had about reached their current position, the Earth experienced a climate optimum, with substantial eustatic sea level rise taking place. In North-western Europe, the *relative* sea level rise was likely to be even larger than elsewhere, because of tectonic subsidence due to the start of the Alpine orogeny along the southern boundary of Eurasia. As a result, the Netherlands became entirely covered by the sea and the predominant sedimentary environment changed from continental (paludal, fluvial and deltaic) in the Early Cretaceous, to (mostly shallow) marine in the Late Cretaceous. Concretely, this means a transition from mainly clays and sands, to glauconitic sand (Aken Formation and Vaals Fm.) and finally to carbonate sand or calcarenite (Gulpen, Maastricht and Houthem Fm.) [Berendsen, 2008]. A graphical representation of this transition is depicted in the figures below. Although the Houthem Formation is not formed during the Cretaceous any more, but instead at the very beginning of the following period, the Palaeogene, it is still part of the Krijtkalk Groep (English: Chalk Group) and generally consists of the same material as preceding formations [Wesselingh et al., 2013]. So, the youngest and last formation of the Cretaceous is the Maastricht Formation.

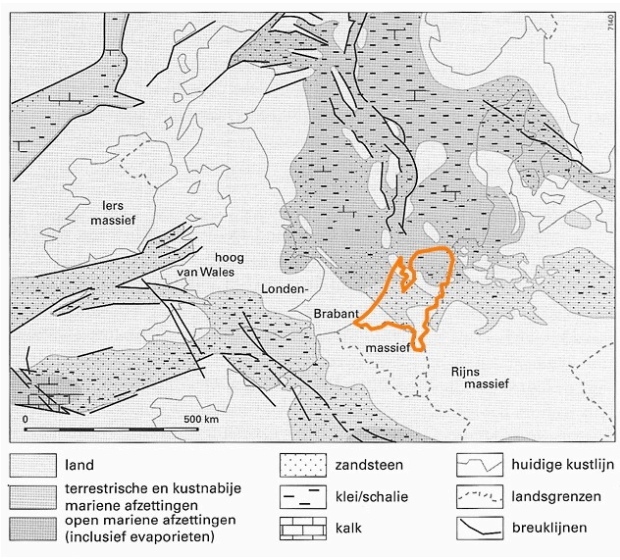

Figure 2: Paleogeography of North-western Europe during the Early Cretaceous, ±130 million years ago. The current borders of the Netherlands are highlighted in orange. Adapted from Berendsen, 2008.

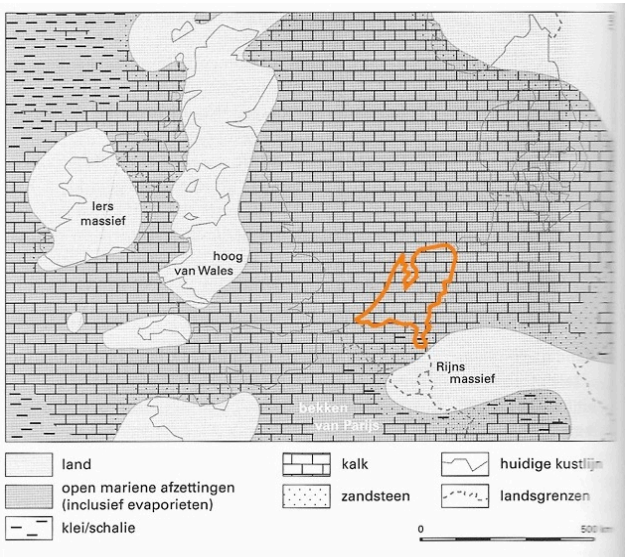

Figure 1: Paleogeography of North-western Europe during the Late Cretaceous, ± 70 million years ago. The current borders of the Netherlands are highlighted in orange. Adapted from Berendsen, 2008.

For this research, the Maastricht Formation is of main interest, as this is the formation in which the A2 highway tunnel is being built. The Maastricht Formation often contains distinct chert nodule concentrations and it is also well known for containing lots of fossils. The size of these fossils varies from small, such as many different kinds of shellfish, to enormous, such as Mosasaurs, thanks to which the Maastrichtian “mergel” became famous not only amongst geologists and palaeontologists [Berendsen, 2008]. A photograph that gives an impression of the fossil content of a split piece of raw Maastrichtian calcarenite, is displayed below (fig. 3).

The Maastricht Formation was formed during the Maastrichtian age, from 72.1 to 66.0 million years ago [International Commission on Stratigraphy, 2013]. As almost every other rock formation, it is also subdivided in members. The uppermost member of the Maastricht Formation is called Meerssen Chalk, which is a relatively coarse-grained calcarenite with very high (>95%) $CaCO_3$-content and which does *not* contain chert nodules [Felder, 1989]. This member has a thickness of up to 20 metres and is underlain by the Nekum Chalk.

The Geusselt section of the A2 tunnel mainly lies within the Meerssen Chalk and for a small part also in the Nekum Chalk. On the sampling location, the boundary between Meerssen and Nekum Chalk is expected only about one metre below the excavation level.

Figure 3: Bed of fossils in a calcarenite from Maastricht [personal photograph, 2013].

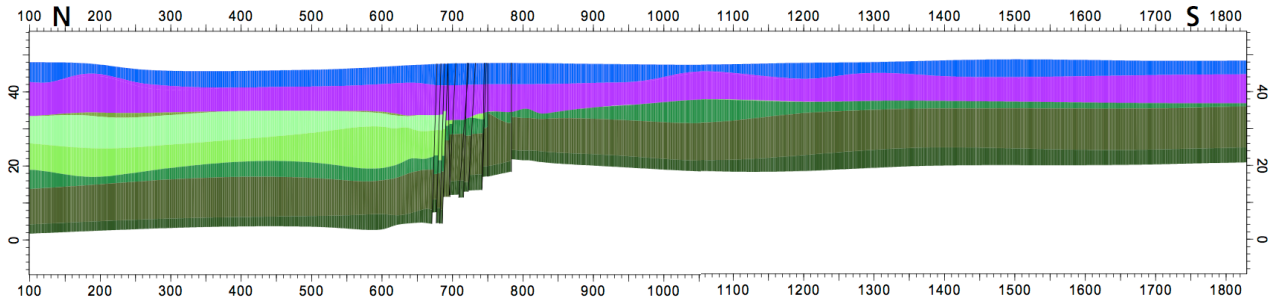

Figure 4: Geological cross-section along the A2 highway track, where members of the Maastricht Formation are coloured green. The Geusselt section is located north (left) of the fault zone. [Kouwenberg, 2009]

2.2 A2 tunnel construction project and geotechnical aspects *

Due to increasing traffic on the A2 highway that ran right through the middle of the city of Maastricht, causing nuisance for residents, local authorities began to think of possible solutions for the developing problem already in the early 1980s. As is often the case, however, most ideas and plans got stuck on financing, such that it lasted until the mid 1990s before the discussion was taken up again, resulting in a "startnotitie" by Rijkswaterstaat in 1995, but still no budget was available. The municipality of Maastricht and the province of Limburg continued to negotiate with the State about the urgent need for a solution, resulting in a "bestuursovereenkomst" (English: management agreement) between the directing parties (the State, the Province and the municipalities of Meerssen and Maastricht) in 2003, with the task to develop a plan of action with durable measures to improve the accessibility, traffic flow through and quality of living in and around Maastricht. Since that time, plans became more concrete, with a preference for the construction of a tunnel. In early 2006, a complementary management agreement was drawn up, containing a cost estimation (€ 631 million), the share of the different parties in this and the required amount of lanes (2 × 4), amongst other boundary conditions. In mid 2006, the study of possible alternatives (expansion of the existing highway over ground, or a bypass around the city) was finished and a definite decision in favour of a tunnel was recorded in the "Trechteringsbesluit Tracé".

By the end of 2006, an open call for tender was issued and, after a selection procedure, on 25 June 2009 the choice for the supposedly best plan for city and highway was announced: the chosen plan is named "De Groene Loper" (English: The Green Strip) by Avenue2, a collaboration between the Dutch partner companies Strukton Civiel Projecten, Stukton Bouw & Vastgoed, Ballast Nedam Infra and Ballast Nedam Ontwikkelingsmaatschappij. In the following months contracts were signed, the definite design ("Tracébesluit") was developed and presented, and the required permits were provided. The contractual budget for the realisation of De Groene Loper amounts to 515 million Euros.

Figure 5: Computer generated cross-section of the stacked tunnel after completion [A2 Maastricht, 2013].

The plan comprises a *stacked* tunnel consisting of two levels, each level containing two separate tubes and each tube containing two lanes, reducing the total traffic load at the surface by 80% compared to the current situation. The upper level will be meant for local traffic, the lower level for continuous or long-distance traffic. The tunnel is going to have a total length of 2.3 kilometres and will be the first stacked tunnel in the Netherlands. At the surface, on the other hand, a new park-like zone with much space for vegetation (the "green strip"), as well as a road for low-speed local traffic and public transport, and paths for cyclists and pedestrians will be laid out. The tunnel is planned to be put into use by the end of 2016 and the whole Groene Loper project (including surface works) is planned to be completed by the end of 2017.

*) Source: A2 Maastricht, 2013, unless defined otherwise.

In 2011, preparation works like the removal and relocation of cables and pipes, and the demolition of buildings were started. In 2012, the real construction works began in the northern part (Kruisdonk section) of the new highway trajectory. The tunnel is being built by means of the *cut-and-cover method* ("open-bouwputmethode"). Depending on the location, the soil conditions and the space that is available, different retaining structures are installed: sheet pile walls and diaphragm (slurry) walls. These walls are temporarily supported by (shuttering) struts or, when the width of the building pit does not allow for placing struts, by deep grouted anchors, to prevent wall collapse after excavation.

A part of the tunnel, however, has to be built by means of the less well-known *walls-roof method* ("wanden-dakmethode") because there is not enough space for the highway and the construction works together. By this method, first reinforced concrete diaphragm walls are constructed. Then, about half of the roof of the final tunnel is built, supported by the soil underneath. Now the highway is relocated on top of this first part of the tunnel roof, creating space to build the opposing diaphragm walls and the remaining part of the roof of the tunnel. Within this concrete container, the soil can be excavated (whilst strutting the roof temporarily) and the tunnel walls and floors are constructed: these works take place underground and will not cause any additional inconvenience for traffic on the surface. When the inner walls are ready, the temporary struts can be removed and the tunnel roof can be finished.

Some particular geo-hazards have to be taken into account during the construction project. In the first place, the rock strength varies from moderately weak and cohesive, to very weak without any cohesion. Moreover, the composition and grain size of the soil vary substantially, from almost pure carbonate sand(stone), to extended fluvial gravel deposits of Palaeogene and Neogene age. This also affects the permeability, so that water can intrude very quickly; especially the risk of local floor uplifting is present [Van Dalen, 2011, and Servais, 2013]. At high water flow rates, due to regular drainage or a calamity, piping could occur, because the less cohesive calcarenite can be washed out easily [Van Dalen, 2011]. Besides, the calcarenite shows local karst phenomena and therefore water flow shortcuts are already present, as well as cavities and small-scale dolines. Soil investigation does not take away these risks, but a sensible design with high safety margins, intensive monitoring and calamity scenarios can limit the risks to a large extent [Van Dalen, 2011]. Therefore, a so-called *observational method* is followed, by which continuous monitoring and review takes place, enabling modifications to be incorporated during construction [Servais, 2013].

Figure 6: Karst phenomena visible at the A2 tunnel construction site [personal photograph, 2013].

3 Materials and methods

In the following sections the used materials and the followed procedures for obtaining the data are described.

3.1 Needle penetration tests

Needle penetration tests were performed on site, on an undisturbed rock outcrop, before cutting sample material for subsequent laboratory work. The location was situated in the Geusselt section of the A2 tunnel in Maastricht. Penetration tests were performed on two different parts of the outcrop, with a distance of about fifteen metres in between (exact GPS coordinates can be found under *Results*).

The apparatus used is a spring-loaded *pocket penetrometer* manufactured by Eijkelkamp, the Netherlands. It does not have a cone, like many other penetration instruments, but a needle of hardened steel instead. The diameter of the needle used was 1.36 mm. Dr. D.J.M. Ngan-Tillard very accurately described the way of utilization in an article as follows:

Figure 7: The spring-loaded pocket penetrometer being used by W. Verwaal [personal photograph, 2013]. The arrows point out rows where penetrations were performed (tiny holes are hardly visible).

"The needle of the Eijkelkamp penetrometer is pushed until a constant compression of the spring is observed or the maximum needle penetration (8.5 mm) is reached. The spring compression is read with the help of an indicator ring on the millimeter scale of the penetrometer. The maximum spring compression is 8.5 cm. By similarity with cone tip resistance, the needle resistance, NPR_E is calculated by multiplying the spring stiffness by the observed spring compression and by dividing the calculated force by the needle cross section. The sensitivity of the Eijkelkamp penetrometer can be optimized by adjusting the spring stiffness. Springs with a capacity of 50, 100, and 150 N are available." [Ngan-Tillard et al., 2011].

For this test on calcarenite, a 50 N spring with a stiffness of 5 N/cm was used. Penetration tests were carried out systematically in horizontal rows with 9-14 measurements per row. The separation between the penetration points was about 2-3 cm and the vertical separation between the rows was 10 cm. Penetrations were performed in horizontal direction, i.e. parallel to the orientation of sedimentary bedding.

After calculating the needle penetration resistance as described by Ngan-Tillard, additionally the unconfined compressive strength (UCS) was estimated by using the following empirical relationship, which has a correlation coefficient (r) of 0.834:

$UCS = 0.0731 \cdot NPR_E$ [Ngan-Tillard et al., 2011]

Estimated UCS values resulting from these calculations are presented in chapter 4 *Results*.

3.2 Unconfined compression tests

Unconfined compression tests were performed in the laboratory of the Department of Geoscience and Engineering within the Faculty of Civil Engineering and Geosciences at Delft University of Technology, the Netherlands. The testing apparatus itself was designed and built by technical and scientific university staff and meets the requirements of ASTM D2938-95 (2002), ASTM D3148-96 and ATSM D4543 standards. The procedure for performing a UCS test is relatively straightforward in terms of control and operation, since measurements are largely automated. There are a few points of attention, however.

Of course, the device should be calibrated properly (which was already done by a technician in this case). Furthermore, the apparatus should ideally be set to constant displacement mode, instead of constant pressure mode to avoid overshooting after failure has occurred. For this project, the apparatus was set up and operated by an experienced technician (A. Mulder), according to the ASTM standards.

The samples for UCS testing were not taken from drilling cores, but from large blocks that were carefully sawed from the outcrop on the construction site by using an electric chainsaw, just after the penetration tests were done. These raw blocks were numbered according to their relative vertical position in situ (for an overview of the numbering, see chapter 4: table 5) and placed in plastic boxes, filled up with loose material for safe transport.

The preparation of ‘cores’ for UCS tests went as follows: an elongated subsample of at least 5 cm in diameter and about twice this size in length was cut from a large raw block by using a hacksaw blade. Cylindrically shaped samples were prepared on a sample trimmer, by turning it around and simultaneously carefully scraping off excess material with a large blade. Be aware that the sample should be cut in such a way, that the width to height ratio lies around 1:2. Since the diameter will be trimmed down to 5 cm, the initial height has to be about 10 cm.

Figure 8: Sample ready for unconfined compression test (with vertical displacement indicators not positioned yet) [personal photograph, 2013].

The most useful information on UCS will be obtained when also the effects of anisotropy are investigated by preparing and testing samples in different directions (i.e. parallel and perpendicular) with respect to the orientation of the sedimentary bedding.

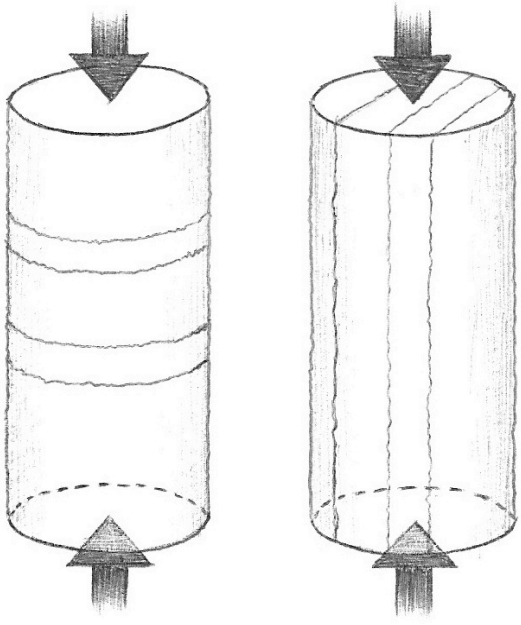

Figure 9: Force direction perpendicular (left) and parallel (right) to the sedimentary bedding orientation [personal drawing, 2013].

3.3 Direct shear box tests

Shear box tests were also performed in the laboratory of the Department of Geoscience and Engineering at Delft University of Technology. The shear box apparatus that was used, is manufactured by ELE-Intertest BV, the Netherlands.

All shear box tests were (supposedly)* performed according to the British Standard (BS) 1377 Part 7 (1990). I would like to kindly refer the reader to that document to learn about the procedure of setting up and performing a direct shear box test in detail, as it covers many pages and it would overshoot the mark to cite all concerning portions of it in this thesis. A summary of the sample preparation procedure and of the shear box test procedure will be given nonetheless.

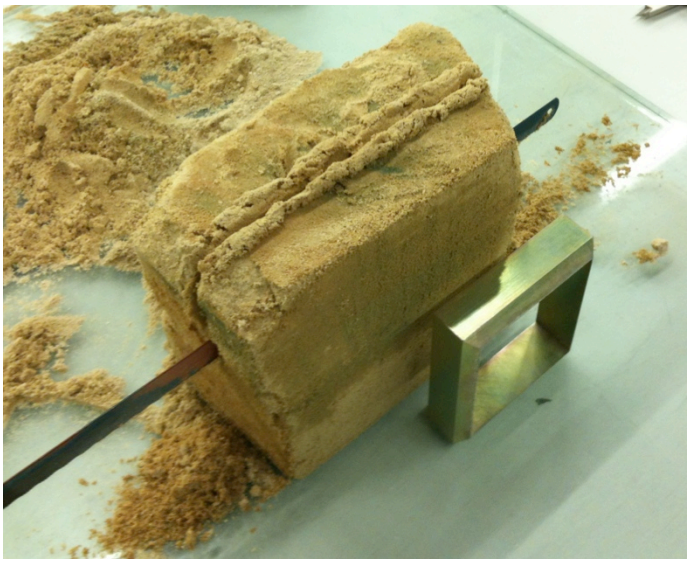

Figure 10: Sawing a slice of calcarenite by using a hacksaw blade [personal photograph, 2013].

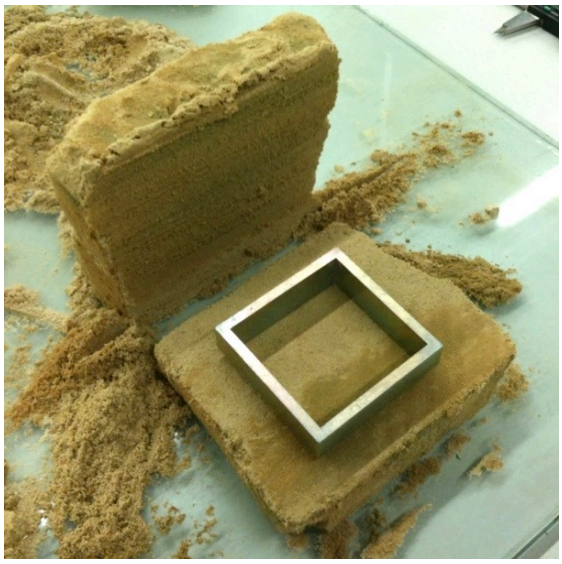

Figure 11: Flattened slice of calcarenite with the cutting mould on top [personal photograph, 2013].

To start with sample preparation, a slice with a thickness of about 3-3.5 cm was cut from the large raw material blocks by using a hacksaw blade. The slice should have a frontal area of *at least* 6.5 × 6.5 cm (though 10 × 10 cm or more is recommended), as the small shear box has inner dimensions of about 6 × 6 cm and there will always be some loss of material. This slice had to be flattened on both sides in order to create flat surfaces, such that the slice would not break apart during cutting by pressure when lying on one side. After flattening, the cutting mould was placed on the upper slice surface and the sample was carefully sawed to be slightly larger than the cutting mould. Then the cutting mould was pushed down by using a *Brazilian tensile strength* testing apparatus in order to achieve a controlled, steady and equally distributed pressure.

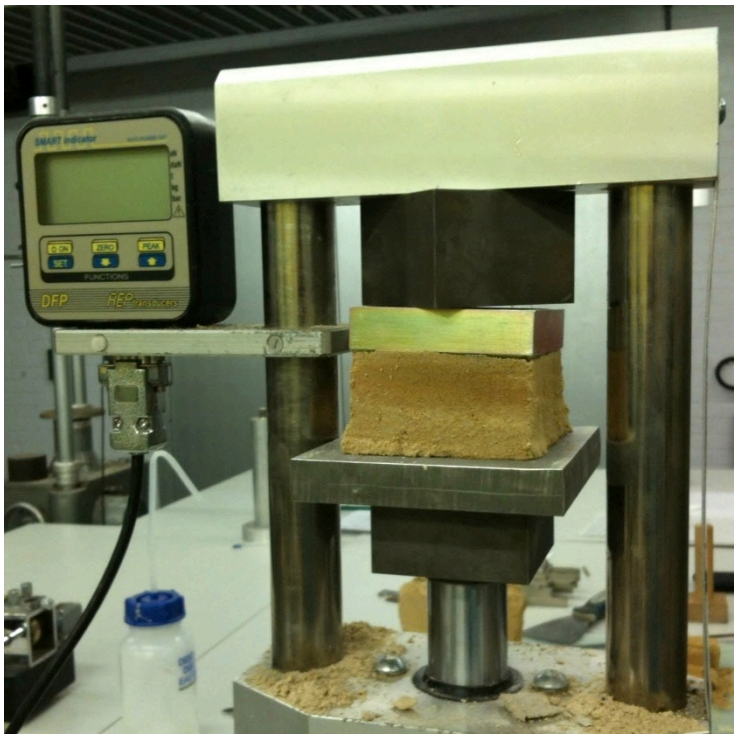

Figure 12: Pushing the cutting mould down by using a Brazilian tensile strength testing apparatus [personal photograph, 2013].

*) Note that for a part of the shear box tests, the British Standard was not followed exactly. Please consult section 5.3 to find out more about why and to what extent my methodology was different from the BS.

The mould is pushed down until it completely encloses the calcarenite sample. Excess material was carefully scraped off by using a reinforced filling knife in order to get (almost) perfectly flat surfaces. The shear box sample enclosed by the cutting mould is weighed to determine the initial (moist) bulk density of the material (after subtracting the mass of the cutting mould itself, of course). 'Waste' material from cutting and scraping was used to determine the moisture content.

Now the sample was carefully pressed out of the mould into the shear box. One should not forget about putting the grooved base plate *and* a porous drainage plate in the shear box already on beforehand [BS 1377 Part 7, 1990]. The shear box is covered by another porous drainage plate and finally by a loading cap and then placed into the shear box apparatus. The confining screws are tightened, whilst shear box alignment screws are removed, and the desired load (normal stress) is applied by using the load hanger positioned on the loading cap. An overview of the applied loads and their calculation is given in table 1 on the next page.

In order to measure the shear force, as well as the horizontal displacement and the average vertical displacement (dilation), three separate digital indicators manufactured by Mitutoyo Corp., Japan, were installed on the shear box apparatus and connected to a computer. The computer was running a measuring application called "mp3", developed by a former TU Delft student, which is able to simply measure digital input from various sources and display the measured values graphically in real time. The shear box testing apparatus was set to a horizontal displacement rate of 0.5 mm per minute and was started together with a new measurement in *mp3*.

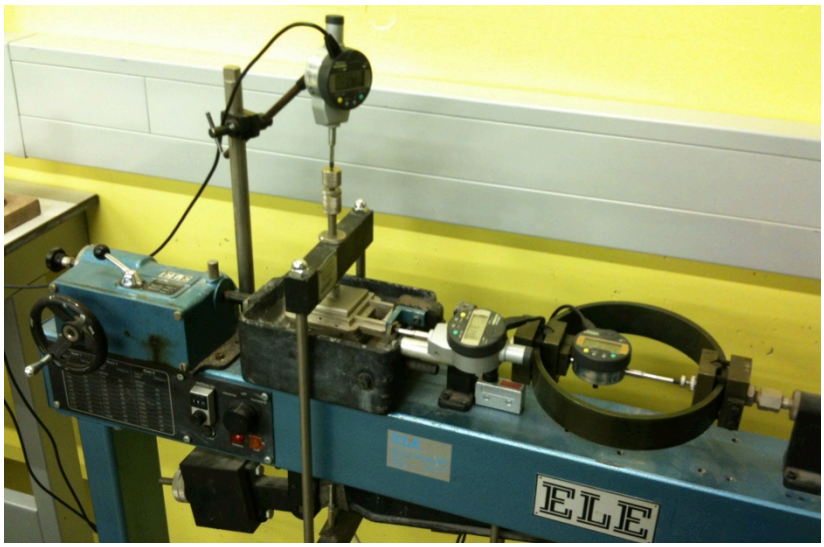

Figure 13: The shear box test apparatus, with the loaded sample in the black container, and all indicators installed [personal photograph, 2013].

Figure 14: Overview of the complete shear box test apparatus, including load hanger with load [personal photograph, 2013].

After shearing, the shear box was turned backwards until no significant shear force was being applied on the sample any more, before taking off the load and untightening the shear box confining screws. The sample was carefully taken out and taken aside, in case it needs to be investigated more closely, e.g. by performing a computed tomographic (CT) scan.

The most useful information on shear strength will be obtained when also the effects of anisotropy are investigated by preparing and testing samples in different directions (i.e. parallel and perpendicular) with respect to the orientation of the sedimentary bedding.

Measurements were processed and plotted in different ways: the force and the vertical dilation were plotted versus the horizontal displacement for each single test. Shear *stress* was calculated by dividing the force with the area of the sample. Also, the maximum shear strength versus the applied normal stress was plotted per series of one particular material and one particular bedding orientation. From these plots, which are also known as "C-phi diagrams", the cohesion or shear strength intercept (S_i) and the friction angle (Φ) could be determined by finding the y-intercept and the inverse tangent of the slope, respectively. Finally, with this information also the unconfined compressive strength (UCS or q_u) was estimated by using the following formula, which can be derived from the Mohr-Coulomb criterion:

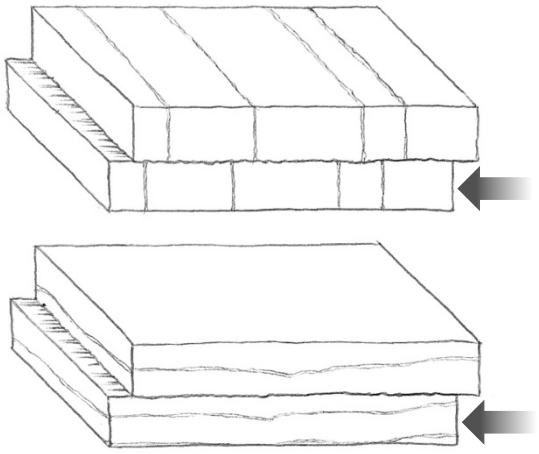

Figure 15: The shear force direction, indicated by an arrow, perpendicular (top) and parallel (bottom) to the orientation of the sedimentary bedding. The upper half of the sample is always fixed; only the lower half is being displaced during a shear box test [personal drawing, 2013].

$q_u = 2S_i \tan(45 + \Phi/2)$ [Goodman, 1989]

UCS values resulting from these calculations are presented in chapter 4 *Results*.

Table 1: Calculated values for normal stress and mass, as well as the really applied amounts of mass and stress. To determine the mass that has to be applied, the normal stress is multiplied by the area of the sample and divided by the gravitational constant g.

	Normal stress S_n	**Mass *m***	***m* applied**	**S_n applied**
Minimum:	60 kPa (1)	21,8 kg / 16,8 kg (2)	17 kg	60,6 kPa
Intermediate:	90 kPa	32,7 kg / 27,7 kg (2)	25 kg	82,7 kPa
Maximum:	120 kPa	43,6 kg / 38,6 kg (2)	35 kg	110,2 kPa
			75 kg (3)	220,3 kPa (3)

Remarks concerning table 1

(1) Based on the minimum normal stress applied during preliminary triaxial tests [Maurenbrecher & Verwaal, 2007].
(2) Excluding load hanger and loading cap (5.03 kg together).
(3) Extended maximum: additional stress for second series of measurements

Note on boundary conditions and other factors influencing shear box test results

At last, it must be remarked that during shear box tests stress and strain distributions are not uniform. Also, the geometry as well as the boundary conditions will change during testing [Allersma, 2005]. Furthermore, Shibuya et al. (1997) have shown that wall friction effects influence the results of direct shear box tests: lubrication of the soil/steel interface was found to be an effective method to reduce these effects. However in this research, which had a rather small time frame, no such lubrication was applied. Moreover, the friction angle is likely to be overestimated in shear tests that show a considerable volume change [Shibuya et al., 1997]. Therefore results from shear box tests should be interpreted with caution.

4 Results

This chapter contains all relevant test results that were obtained on site (needle penetration) and in the laboratory (unconfined compression and direct shear). The results are more thoroughly analysed and discussed in chapter 5.

4.1 Needle penetration tests

In table 2, the measured spring compressions (average, minimum and maximum of multiple readings) are presented. Table 3 lists the penetration resistances calculated from the compressions. On the next page in figures 16 and 17, the resistances are plotted versus depth, including the depth intervals of the raw sample blocks for lab testing. After that, in table 4 the UCS estimations are presented and finally in table 5 the numbering and depths of the raw sample blocks for laboratory testing are given.

Date of site visit: 5 September 2013
Altitude of top of excavated soil layer: +35 m NAP

Location 1 coordinates: 50°51'28''N, 5°42'46''O (GPS), or 50.857833,5.712832 (Google Maps)
Location 2 coordinates: 50°51'29''N, 5°42'45''O (GPS), or 50.857965,5.712689 (Google Maps)

Table 2: Measured spring compression of pocket penetrometer (all units in cm).
Depth is measured from top of excavated soil layer.

Location 1				**Location 2**			
Depth	**Average**	**Min.**	**Max.**	**Depth**	**Average**	**Min.**	**Max.**
40	2,77	0,0	5,8	7	7,82	7,0	8,5
50	4,07	2,8	5,0	16	6,92	5,4	8,4
60	3,71	2,8	5,0	27	8,14	7,1	8,5
70	5,34	4,2	6,7	47	7,60	6,4	8,5
80	4,93	3,8	6,3	57	8,30	7,5	8,5
90	2,67	2,0	3,4	67	7,12	5,0	8,5
100	4,86	3,1	6,8				
110	4,40	2,4	6,9				
120	6,48	5,1	8,0				
130	6,87	5,6	7,8				

Table 3: Calculated needle penetration resistance. Depth is measured from top of excavated soil layer.

Location 1				**Location 2**			
Depth [cm]	**Average [MPa]**	**Min. [MPa]**	**Max. [MPa]**	**Depth [cm]**	**Average [MPa]**	**Min. [MPa]**	**Max. [MPa]**
40	9,52	0,00	19,96	7	26,92	24,09	29,26
50	14,01	9,64	17,21	16	23,81	18,59	28,91
60	12,77	9,64	17,21	27	28,02	24,44	29,26
70	18,39	14,46	23,06	47	26,16	22,03	29,26
80	16,97	13,08	21,68	57	28,57	25,81	29,26
90	9,19	6,88	11,70	67	24,50	17,21	29,26
100	16,73	10,67	23,41				
110	15,14	8,26	23,75				
120	22,31	17,55	27,54				
130	23,63	19,27	26,85				

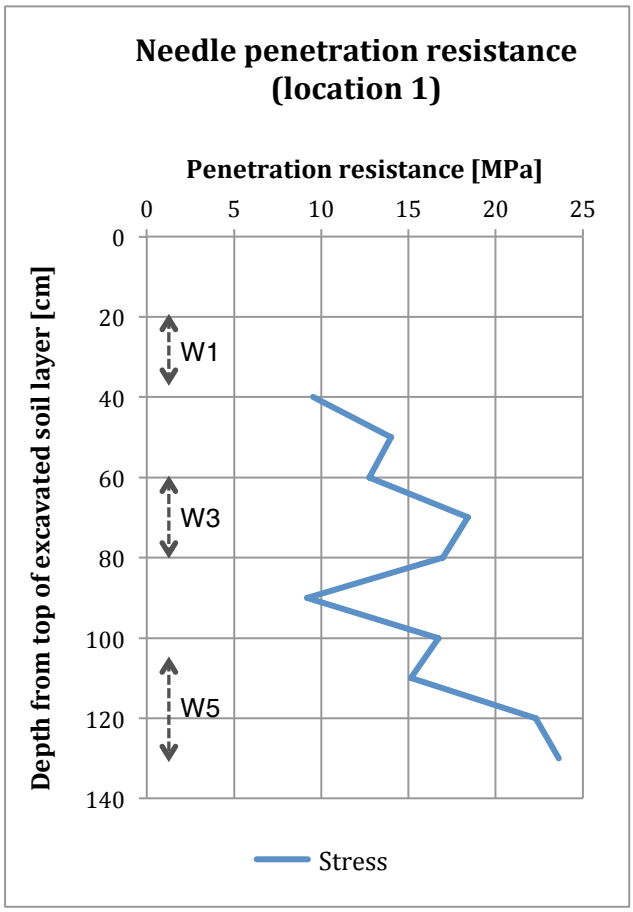

Figure 16: Plot of penetration resistance vs. depth at location 1, including sampling intervals (see table 5).

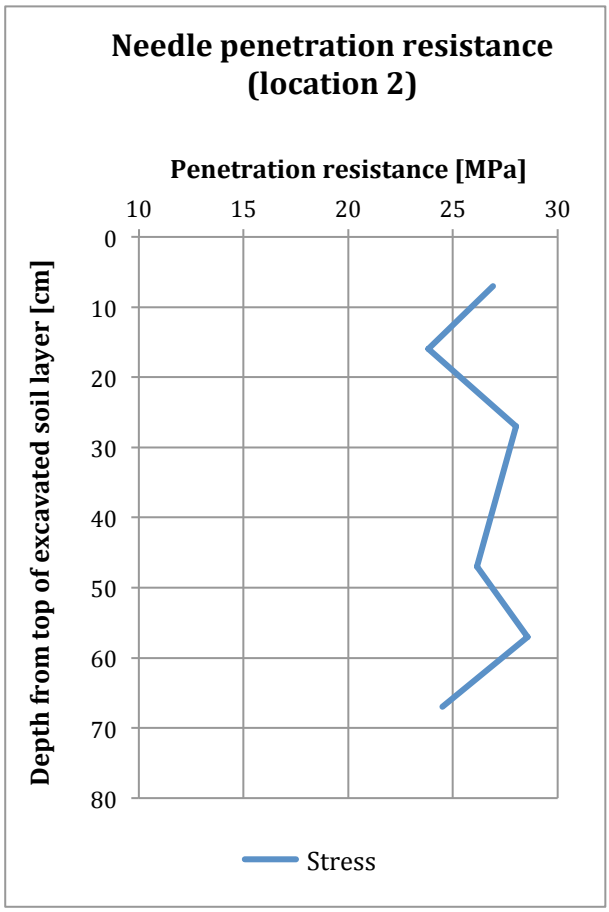

Figure 17: Plot of penetration resistance vs. depth at location 2.

Table 4: Unconfined compressive strength, calculated from needle penetration resistance by using empirical relationship [Ngan-Tillard et al., 2011]. Depth is measured from top of excavated soil layer.

Location 1				**Location 2**			
Depth [cm]	**Average [MPa]**	**Min. [MPa]**	**Max. [MPa]**	**Depth [cm]**	**Average [MPa]**	**Min. [MPa]**	**Max. [MPa]**
40	0,70	0,00	1,46	7	1,97	1,76	2,14
50	1,02	0,70	1,26	16	1,74	1,36	2,11
60	0,93	0,70	1,26	27	2,05	1,79	2,14
70	1,34	1,06	1,69	47	1,91	1,61	2,14
80	1,24	0,96	1,59	57	2,09	1,89	2,14
90	0,67	0,50	0,86	67	1,79	1,26	2,14
100	1,22	0,78	1,71				
110	1,11	0,60	1,74				
120	1,63	1,28	2,01				
130	1,73	1,41	1,96				

Table 5: Numbering and location of the raw sample material.
Interval depth is measured from top of excavated soil layer.

Location 1	Coordinates: 50°51'28"N, 5°42'46"O (GPS), or 50.857833,5.712832 (Google Maps)	
Interval [cm]		
0-20	lost	
20-35	W1	(tested on shear strength)
35-55	W2	
55-60	lost	
60-80	W3 a + b	(tested on shear strength)
80-105	W4	
105-130	W5	(tested on shear strength)

Location 2	Coordinates: 50°51'29"N, 5°42'45"O (GPS), or 50.857965,5.712689 (Google Maps)
Interval [cm]	
0-35	number unknown
35-40	lost
40-67	number unknown

4.2 Unconfined compression tests

For this research only one material was tested on UCS, namely W1 (the uppermost block from the outcrop). This is because of the strict time limitations for a Bachelor project and because this research project focuses on shear box testing and comparison with previous results.

In total, four unconfined compression tests were performed: twice with the sedimentary bedding oriented parallel to the principal (compressional) stress direction, and twice with the bedding oriented perpendicular to the principal stress direction. The reading interval was set to 0.01 mm and the loadcell type used was 50 kN.

In figure 18 the stress/strain curves are displayed together. Table 6 lists the numerical values for UCS and stiffness that result from these curves, as well as the observed modes of failure. The stiffness (E_{50}) is the slope of the tangent line to the stress/strain curve at 50% of the peak strength. Finally in table 7 the dimensions of the tested samples are given.

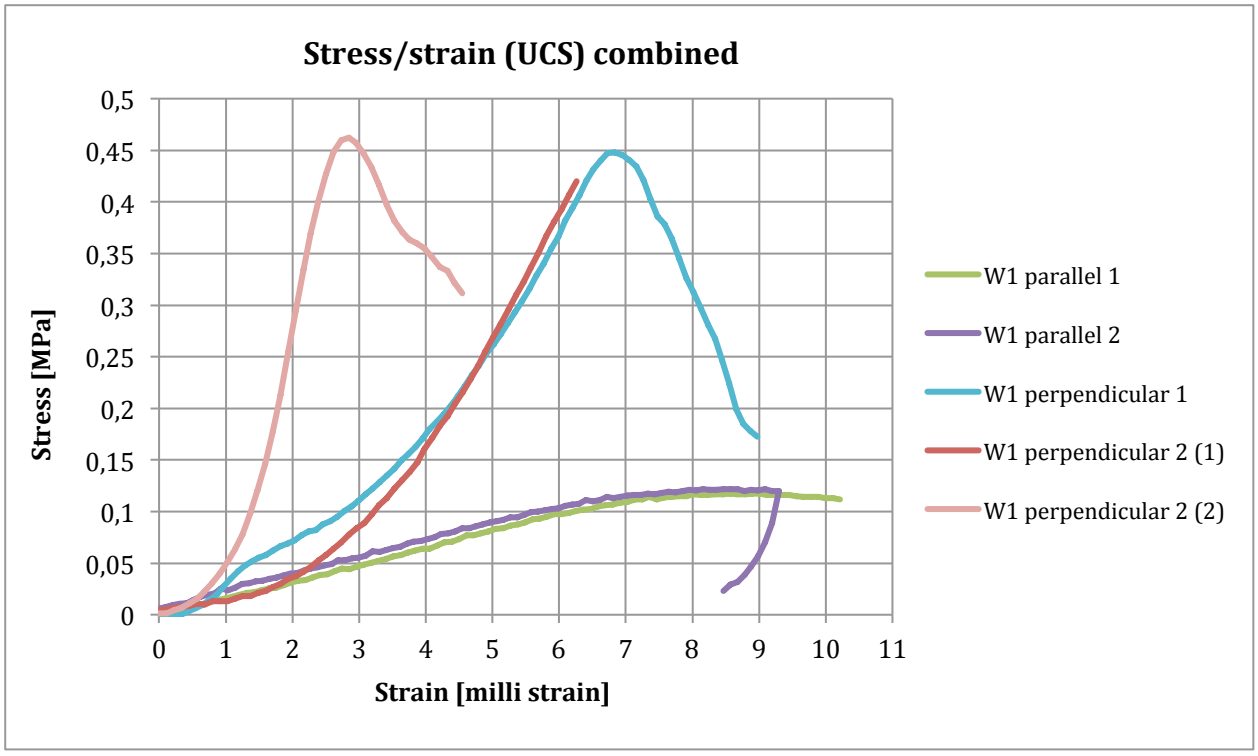

Figure 18: Stress/strain curves for UCS determination of material W1. Note: test *W1 perpendicular 2 (1)* was interrupted because the vertical displacement indicators were pushed in completely. The test was resumed on the same core, which shows a higher stiffness (E), however.

Table 6: Unconfined compressive strength, stiffness (E_{50}) and observed mode of failure.

	UCS [MPa]	E_{50} [GPa]		Mode of failure
W1 parallel 1	0,117	0,017		Vertical (parallel to bedding)
W1 parallel 2	0,122	0,015		Vertical (parallel to bedding)
W1 perpendicular 1	0,448	0,010		Subvertical
W1 perpendicular 2	0,462	0,120 *(1)*	0,319 *(2)*	Subvertical

Table 7: Dimensions of UCS tested samples.

	Diameter [mm]	Height [mm]
W1 parallel 1	49,17	91,40
W1 parallel 2	49,54	97,28
W1 perpendicular 1	49,95	95,29
W1 perpendicular 2	49,30	88,16

4.3 Direct shear box tests

Three different materials (W1, W3 and W5) were tested on their shear strength, each of which at four different normal stresses and also in two different directions (i.e. parallel and perpendicular) with respect to the orientation of the sedimentary bedding. That makes 24 shear box tests together. Several of them were done twice, however (see section 5.3 for discussion), such that in total 32 shear box tests were performed.

Table 8 lists the measured maximum shear stress, or shear strength, of each single test. In tables 9 and 10 the cohesions, friction angles and estimated UCS are given, for the first and second series of tests separately. The friction angles and cohesions were derived from C-phi diagrams, which are shown in figures 19 and 20. Also some images resulting from micro-CT scans are presented in figures 21-25. All less relevant results, such as (combined) plots of shear stress and vertical dilation vs. horizontal displacement can be found in Appendix C.

Table 8: Shear strengths (S_{shear}) (all units in kPa). The first series of tests is marked by a light grey colour.

	Normal stress	**S_{shear} parallel**	**S_{shear} perpendicular**
W1	61	81,9	101,2
	83	103,0	123,6
	110	124,5	180,4
	110 (2)	141,9	184,0
	220	209,1	252,0
W3	61	77,0	83,7
	61 (2)	86,0	169,7
	83	92,2	
	110	104,8	170,6
	110 (2)	149,5	191,6
	220	227,4	292,3
W5	61	75,2	140, 6
	83	112,4	205,5
	110	124,9	181,8
	110 (2)	150,9	208,2
	220	230,1	287,8

Table 9: Cohesions, friction angles and estimated UCS (Mohr-Coulomb) for the *first* series of tests at normal stresses of 61, 83 and 110 kPa.

	Cohesion [kPa]		**Friction angle [°]**		**UCS [kPa]**	
	parallel	perpendicular	parallel	perpendicular	parallel	perpendicular
W1	29,9	0	40,9	57,7	130,6	0
W3	43,7	0	29,4	56,5	149,4	0
W5	20,0	110,2	44,8	37,8	96,3	450,1

Table 10: Cohesions, friction angles and estimated UCS (Mohr-Coulomb) values for the *second* series of tests at normal stresses of 61 kPa (2), 110 kPa (2) and 220 kPa.

	Cohesion [kPa]		**Friction angle [°]**		**UCS [kPa]**	
	parallel	perpendicular	parallel	perpendicular	parallel	perpendicular
W1	74,8	115,9	31,4	31,7	152,4	384,6
W3	42,3	114,1	40,7	38,5	230,4	414,2
W5	71,6	128,5	35,8	35,9	176,7	339,9

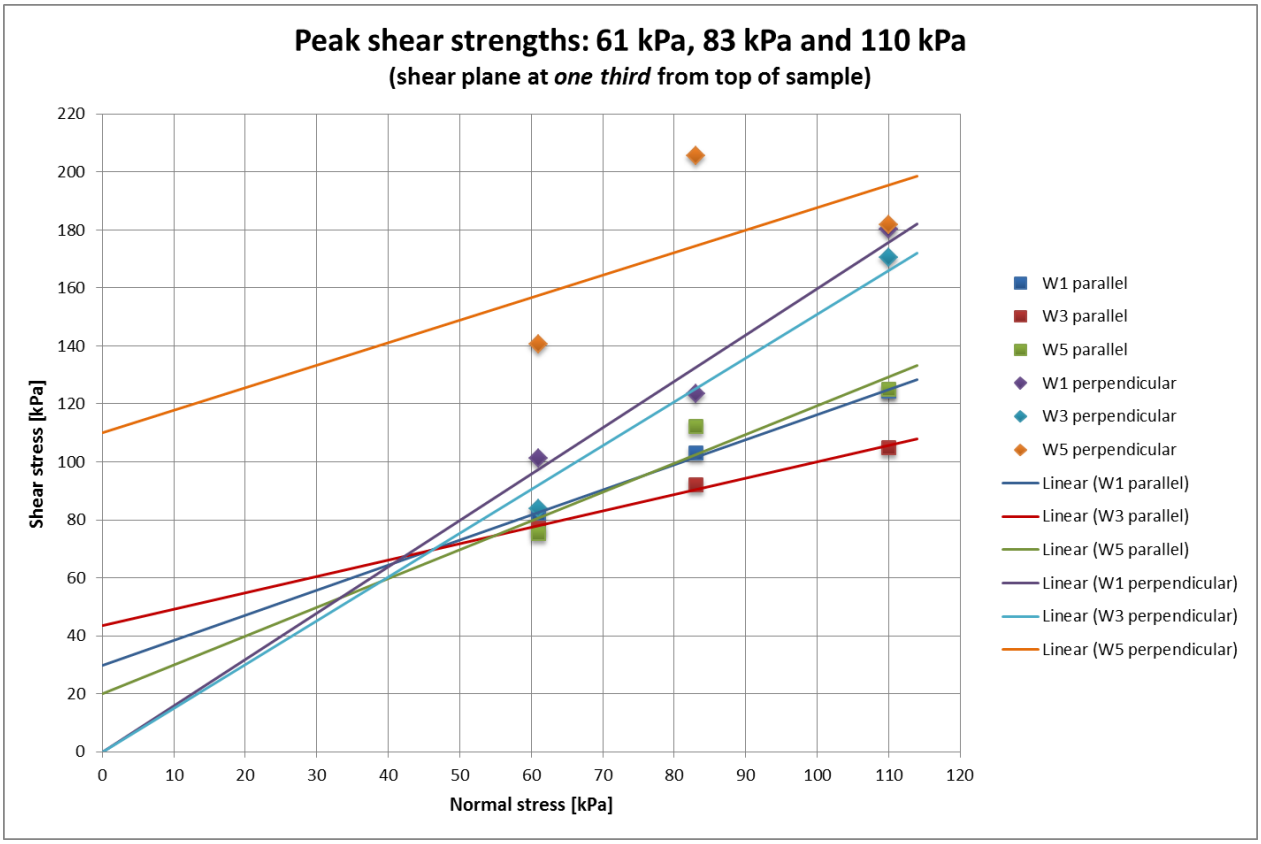

Figure 19: Shear strength vs. normal stress (C-phi diagram) for the *first* series of tests, with linear trend lines.

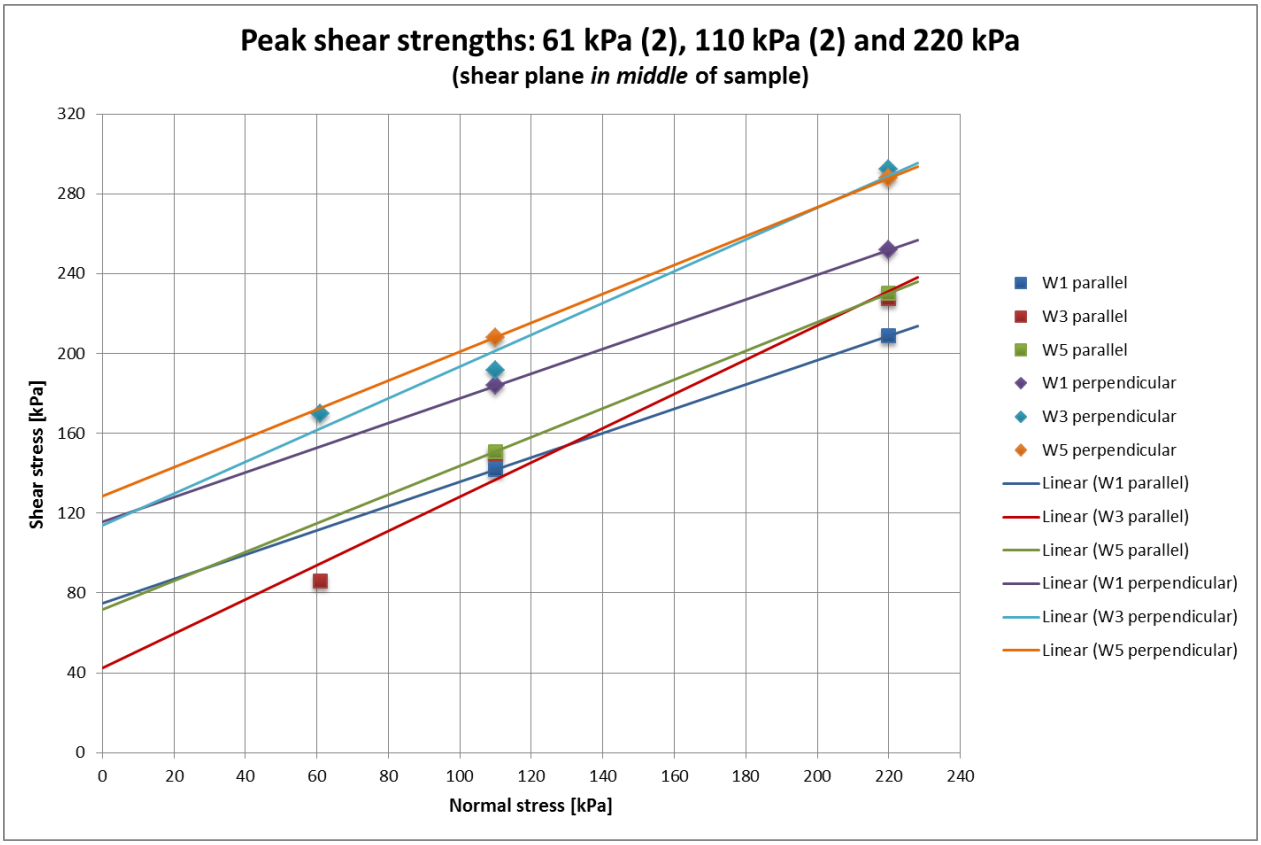

Figure 20: Shear strength vs. normal stress (C-phi diagram) for the *second* series of tests, with linear trend lines.

Below, some images that resulted from micro-CT scans are presented. Such scans were done in order to visualize the deformation patterns in 3D. The white arrows indicate the direction of the shear force, as well as the part of the sample that had moved: the upper half of a sample is always fixed, only the lower half is being displaced during a shear box test.

In the first four images, areas of low density appear dark and areas of higher density have a lighter colour. In the last image the colour scheme is inverted, thus showing areas of high density in a darker colour than less dense areas. Sample dimensions: width × height = 6 × 2 cm.

Figure 21: Micro-CT cross-section (side view) of a sheared sample from the first test series, where the shear plane was at 1/3 of the sample height from the top (see discussion). The material displayed is W5 parallel, tested at a normal stress of 83 kPa.

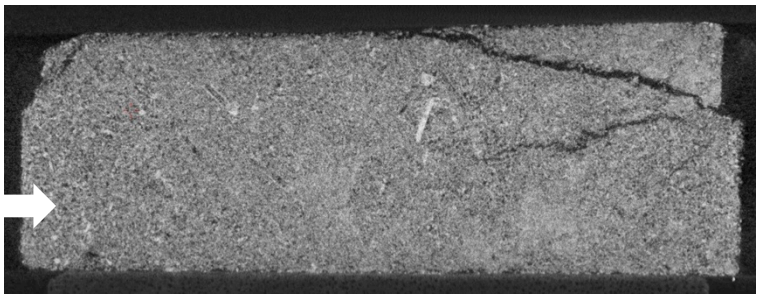

Figure 22: Micro-CT cross-section (side view) of the same sample as figure 20, but dissected at a different location.

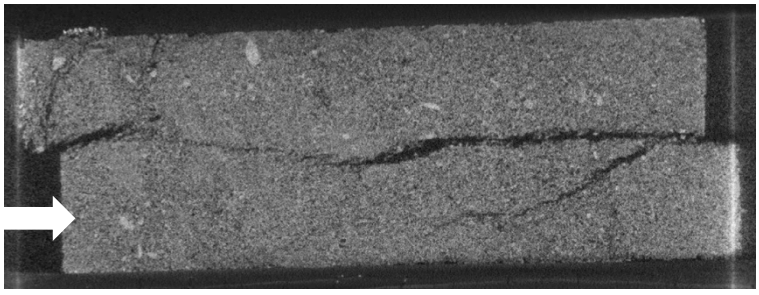

Figure 23: Micro-CT cross-section (side view) of a sheared sample from the second test series, where the shear plane was (correctly) at 1/2 of the sample height. The material displayed is W5 parallel, tested at a normal stress of 110 kPa.

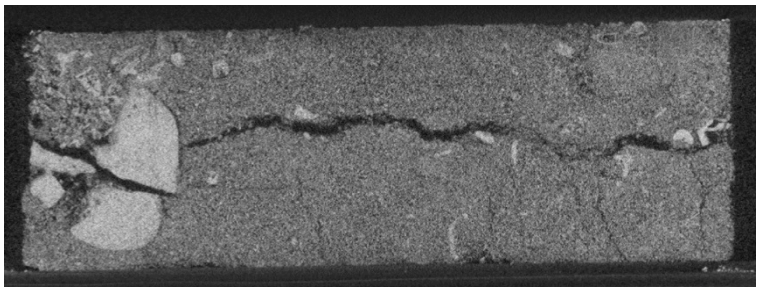

Figure 24: Micro-CT cross-section (front view) of the same sample as figure 23.

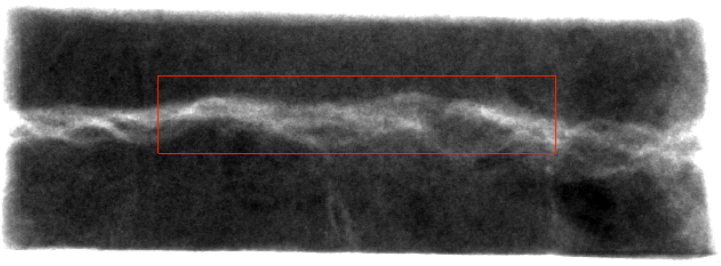

Figure 25: Micro-CT trans-illumination (front view) of the same sample as figures 23 and 24.

5 Analysis and discussion of results

5.1 Needle penetration tests

The first thing that strikes from the needle penetration (NP) test results is the substantial variation of compression readings within a row at constant height. The difference between minimum and maximum readings amounts to about a factor 2, sometimes even more. Results from NP generally show such high variation, because the penetration area is very small and, as a consequence, highly sensitive to small-scale inhomogeneities – keeping in mind that, depending on the location, inhomogeneities like fossils of several millimetres to centimetres in size are abundant (see also figure 3 in section 2.1). Therefore multiple readings per depth level were done, in order to get representative mean values.

Regarding the means or averages, a trend towards increasing strength (NP resistance from 9.5 to 23.6 MPa) with increasing depth is observable on location 1. This was more or less expected, as deeper material is less exposed to weathering and probably also less disturbed by excavation works. A trend like that could not be observed on location 2: here the NP resistance is more constant, but considerably higher in general (between 23.8 and 28.6 MPa).

The estimated unconfined compressive strengths (UCS) that were calculated from the needle penetration resistances by using an empirical relationship [Ngan-Tillard et al., 2011] are roughly a factor of 10 higher than those obtained by UCS testing. Such a large difference is somewhat unexpected. The modes of failure for NP and UCS are very different, however: during unconfined compression tests samples fail by axial splitting (tensile failure), whilst during NP tests grain crushing occurs (compressive failure). This might largely explain the differences between estimated and measured UCS. Furthermore, since the total number of NP readings was rather small (9-14 measurements per depth interval), the accuracy of the UCS estimation may also be lower, which is already pointed out by Ngan-Tillard et al. (2011): “when a limited number of tests are done on the same material, the needle penetrometer test is recommended as an index test rather than a way to determine accurately the UCS of the Maastrichtian limestones”.

5.2 Unconfined compression tests

Concerning the unconfined compressive tests, there is not so much source for discussion. Some interesting observations can be made nonetheless. In the first place, it is evident that the UCS strongly depends on the direction of the principal (compressive) stress with respect to the orientation of the sedimentary bedding: UCS differs by a factor of 3.75 between parallel (about 120 kPa) and perpendicularly (about 450 kPa) tested samples. For anisotropic (layered) sedimentary rocks, such a significant difference is not rare, however.

Considering each bedding orientation separately, the consecutively obtained UCS values lie very close together: 117 vs. 122 kPa (parallel) and 448 vs. 462 kPa (perpendicular), all of the same material (W1). So the obtained results are repeatable.

Furthermore, it should be mentioned that one of the tests was interrupted just before peak strength was reached, because the displacement indicators had to be repositioned. After repositioning, the test was carried out again on the same sample, but a significantly steeper curve could be observed. Since the slope indicates the stiffness (E) of the material, this value is therefore higher for the resumed test. Note that single-cycle E values correspond to the total stiffness, whilst E values resulting from compression tests that incorporate one or more unloading/reloading cycles correspond to the modulus of elasticity, or Young’s modulus of the material [Ngan-Tillard, pers. comm., 2013]. An increasing E is very commonly observed behaviour for multi-cycle compression tests [Oliveira et al., 2006]. Single-cycle E values of 15 and 17 MPa (parallel), as well as 100 and 120 MPa (perpendicular) were obtained. Unloading and reloading caused the E to increase by a factor of 2.6.

5.3 Direct shear box tests

Unfortunately, a large portion of the performed shear box tests did not go, as it should go. The reader will have noticed that shear box test results are divided in different “series”: a first series in which samples have been tested at normal stresses of 61, 83 and 110 kPa, and a second series in which samples have been tested at 61, 110 and 220 kPa. Additionally, also a series where all test results are put together was evaluated (see Appendix C part 1). This complicated separation had to be made because the first complete series (61-110 kPa) was not tested according to the British Standard (BS). Since only one porous drainage plate was available in the testing laboratory, we thought that this would likely cause no problems, as we were testing highly porous and unsaturated material, where no water would be released and pore pressures would not increase too much. But by leaving out one (the lower) drainage plate, the sample was also lying lower in the shear box. On its own, this would not have been much of a problem either, but as a result, the shear stress became concentrated on the upper third of the sample. This caused no continuous shear plane to develop along the interface between the two shear box halves, but instead only a wedge-shaped piece to break out. This unexpected mode of failure was only discovered after a few samples were scanned with a micro-CT scanner (fig. 21 and 22). Since the first series of shear box tests yielded quite inconsistent results that were moreover not comparable with previous investigations, practically everything had to be done all over again.

Now that we had gained some experience and thought that the chosen normal stresses were too low, which might have also been of influence on the development of the shear plane, we decided to double the maximum applied load, besides testing on 110 kPa again to see what the difference was compared to the first series. Thus every material was tested again at two orientations and at two different normal stresses. In addition, one material (W3) was also tested at the lowest normal stress of 61 kPa again. The newly obtained data looked a lot more consistent and also a continuous shear plane developed (fig. 23-25): this was the case for every test where the sample was positioned correctly in the middle of the shear box, i.e. when the mid-plane of the sample coincides with the interface between the two shear box halves. From these results, it could be deduced that the applied normal stress (within the chosen range) does *not* influence the development of the shear plane. Instead, *correct positioning* of the sample is the most important condition for the development of a horizontal shear plane.

By knowing that the first shear box test series was not performed according to the BS, which resulted in inconsistent data, I would recommend to disregard these results entirely. By doing so, only the second series of tests remains, which is a (too) small number of valid results, however.

From the C-phi diagram (fig. 20) it can be visually ascertained that there is a clear difference between parallel vs. perpendicularly tested samples: just as with UCS, the perpendicularly tested samples are significantly stronger. Furthermore, a weak tendency towards increasing strength from W1 to W5 is observable: W1 mostly has the lowest shear strength at failure, as was already expected from the visual inspection of the material. Cohesions were found to range from 42.3 kPa (parallel) to 128.5 kPa (perpendicular).

Friction angles range from 31.4° to 40.7° with *no* significant difference between parallel and perpendicular. Whereas cohesions are proportional to shear strength, friction angles do not show any proportionality with strength, nor with depth. It can only be observed that material W3 has the highest friction angles (up to 40.7°), whilst showing the lowest cohesions. In the course of testing, it was already noticed that W3 was the most inhomogeneous and most coarse-grained material, containing lots of fossils. W1 on the other hand, has the lowest friction angle and was considered to be the most homogeneous and least coarse-grained material; W5 was intermediate with respect to the others. Therefore, one could cautiously conclude that more inhomogeneous or coarser grained materials have a higher friction angle. This seems to be in accordance with existing literature [Douglas, 2002], stating that an increase of the *ratio of maximum particle size to sample diameter* also causes the (secant) friction angle to increase.

Considering the estimated UCS, which were calculated from shear strength data (c and Φ) by using a formula derived from the Mohr-Coulomb criterion [Goodman, 1989], one could say that this gives a fair approximation when compared to the real UCS: the estimations gave UCS of 152 kPa (parallel) and 385 kPa (perpendicular) versus directly measured UCS of about 120 kPa and 450 kPa, respectively. Still, the estimation is different from real UCS by as much as 25% (too high) for parallel tested samples and about 15% (too low) for perpendicularly tested samples. Since the UCS dataset is very limited because just one material (W1) was tested on UCS, only this particular material could be regarded for comparison.

The moisture content of the shear box tested samples varied within a reasonable range. The moisture contents are listed in Appendix E, which shows that they range from 9.32 to 10.81% for W1, from 12.16 to 16.18% for W3 and from 12.62 to 14.60% for W5. It is remarkable that W1 clearly had the lowest moisture content, which can be explained by the fact that this was the uppermost material in situ, from which more water had already evaporated. On this occasion it must be emphasized that moisture content is of utmost importance for the cohesion and general strength of this rock type, being (very weak) calcarenite: it could be observed that after some time (2-3 days) had passed and all the water had evaporated from the tested samples, they had almost no cohesion anymore. A gentle push by the finger or even just some vibrations on the table caused the dry samples to fall apart completely. Surface tension likely is a determining factor for keeping the grains together.

Along with the moisture content, the bulk densities were determined and, subsequently, also the degree of saturation. Bulk densities of the partially saturated samples vary from 1.30 to 1.52 g/cm^3 and are approximately proportional to the moisture content. The total degree of saturation lies between 20 and 41%, for which a specific gravity of 2.72 g/cm^3 was assumed [Ngan-Tillard et al., 2011].

In order to calculate the saturation, also the void ratio had to be determined, which gave somewhat exceptional (high) values, indicating porosities of more than 50%. This required a closer look, but after a quick literature inspection, it was found that “calcareous sands are unique in terms of particle characteristics, including mineralogy, shape, surface texture, high void ratio, and intra-porosity” [Sandoval & Pando, 2012]. Consequently, void ratios as high as 2 and even higher are not uncommon at all [Lavoie & Bryant, 1993, and Lavoie, 1988].

Finally, the last point of discussion concerns the shape of the shear force curves (Appendix C part 2 and 3). On almost every curve a small plateau at about one fourth to one third of the maximum shear strength could be observed. We tried to figure out what this could mean and after a shear box test on remoulded sand, which did not show this characteristic behaviour, we believe to have found the answer: the cutting mould for preparing shear box samples has slightly smaller inner dimensions than the shear box itself (difference ≈ 1-1.5 mm). This makes the sample fit more easily into the box, but leaves a barely visible gap around it. When the shear box apparatus is turned on, first the force increases as the shear box experiences the resistance from the sample that is held down by a load (normal stress). But at a certain level, the force exceeds the (static) friction between the sample and the baseplate of the shear box. At that moment, the sample starts to slide as a whole and consequently closes the ‘gap’. When the gap is closed, the sample is in touch with the walls of the shear box again and the force can increase further until failure (shearing) occurs.

Now the question arose: is this friction force something to be eliminated or subtracted from the total shear force and, subsequently, from the shear strength? After lively discussion we agreed that the force needed to overcome the friction is also working on the sample, therefore contributing to the total stress experienced by the sample and thus being an essential part of the total shear strength. For comparison with existing data, any sort of ‘correction’ for friction would not be useful either, since this was never done before. So, no correction is required. For completeness, all shear box test results including subtraction of the sliding friction can be found in Appendix D, but they are in fact irrelevant and have to be considered as not representative.

6 Comparison with data from preliminary investigations

The following comparison relates entirely to the *Description of core and gravel samples and the determination of geotechnical parameters* by Maurenbrecher & Verwaal, 2007.

For the *Description of core and gravel samples (…)* (to be abbreviated with "DCGS"), several boreholes were drilled, sampled and tested. The boreholes are located along the A2 highway, spanning a large lateral distance. Since rock strength properties are known to vary widely from place to place in this area, to a great extent because of solution (karst) phenomena but also because of fault zones [Servais, 2013], results from boreholes that are situated far from the investigated location are likely to differ a lot. Therefore, for comparison the emphasis will be on nearby boreholes (see also Appendix B part 1): the most nearby borehole is BK07k02, at a distance of only about 30 m from the sampling location, followed by BK07k01, at a distance of about 120 m from the sampling location.

Shear box tests were only performed on location BK02k05, unfortunately not situated very closely to the sampling location. Also, just three tests are performed, resulting in only one C-phi diagram (Appendix B part 2). Since a whole series of shear box test results has to be compared with this single diagram, the significance of this comparison is doubtful. Nevertheless, the DCGS friction angle (36.8°) corresponds very well to the *average* friction angle that was found in the course of this research: 36.6°. The cohesion is poorly comparable though, as in DCGS *no* cohesion was found, whilst the actual research gave very different (nonzero) cohesions, ranging from 42.3 kPa (parallel) to 128.5 kPa (perpendicular).
Note that in DCGS no information is given regarding the orientation of the sedimentary bedding, which proved to be of significant influence.

Then a larger set of triaxial test results is given in DCGS (Appendix B part 2). Of this set, only B07k02 is to be taken into serious consideration; B07k01 was not tested, apparently. Friction angles for location B07k02 amount to 43.9° and 37.1°, which is relatively high (also when compared to the friction angle obtained by shear box tests on material from BK02k05), but still reasonably close to the *average* results from the actual research. Found cohesions, on the other hand, amount to 11 and 59 kPa, whilst my results show cohesions that are generally higher than 70 kPa, with one outlier of 42 kPa. So, cohesions obtained by triaxial tests differ significantly from own results: this counts for most cohesions from triaxial tests on material from other boreholes as well.

Finally, the unconfined compressive strength (UCS) results are to be compared. Whereas the DCGS contains large amounts of UCS data, the actual research yielded only a very narrow dataset. But again, emphasis is mainly on the first two boreholes: on these locations UCS range from 31 to 2280 kPa in the DCGS, which is an extreme spread. If other boreholes would also be taken into account, results deviate even more, with UCS reaching up to 7720 kPa.

When looking only at depths of about 12-15 m below the natural surface, from which the material in my research originated, it seems that the spread in UCS from the DCGS is smaller, with values ranging from 53 to not more than 970 kPa (both in B07k03). The closest borehole with UCS-tested material from this depth interval is B07k01 (at about 120 m distance), giving UCS of 560 and 820 kPa. Still, however, the results from the DCGS generally show no reasonably good correspondence with UCS that were obtained during my research.

The wide spread in strength data from the DCGS could be explained by the fact that the material was damaged due to the rotary core drilling. For very weak rocks and soils, rotary core drilling is a rather violent sampling method, likely causing the microstructure of the material to be damaged and consequently the cohesion to be significantly reduced. Moreover, when also gravel layers or chert nodules are penetrated, these are very likely to crush the surrounding weak calcarenite. Besides, karst phenomena are known to be present and drilled cores might include such zones, whilst for the actual research only intact and undisturbed sample blocks were taken and tested.

7 Conclusions

The analysis of the data resulting from needle penetration, unconfined compression and shear box tests on Maastrichtian calcarenite, led to the following conclusions:

Needle penetration tests:

- Needle penetration readings vary widely due to small-scale inhomogeneities, therefore many readings must be done in order to get representative mean values;
- Needle penetration resistances range from 9.5 to 23.6 MPa on one location and from 23.8 to 28.6 on another location in the vicinity, tested on the same material on similar depths;
- The needle penetration resistance tends to increase slightly with depth, probably because deeper material is less exposed and less disturbed by excavation works;
- The estimation of unconfined compressive strength (UCS) by using an empirical relationship [Ngan-Tillard et al., 2011] did not give satisfactory results that correspond with actually measured UCS values, mainly because of differences in the mode of failure between UCS (axial splitting: tensile failure) and NP (grain crushing: compressive failure).

Unconfined compression tests:

- Anisotropy due to sedimentary bedding is proven to strongly affect the UCS;
- UCS of the investigated calcarenite amount to 0.12 MPa and 0.45 MPa, with principal stress direction oriented parallel and perpendicularly to the sedimentary bedding, respectively;
- Stiffness values are 16 MPa (parallel) and 110 MPa (perpendicular) on average;
- A pre-peak unloading/reloading cycle causes the stiffness (modulus of elasticity) to increase by a factor of about 2.6.

Shear box tests:

- Anisotropy due to sedimentary bedding significantly affects shear strength and cohesion;
- Cohesions of the investigated calcarenite range from 42 to 75 kPa (parallel) and from 114 to 128 kPa (perpendicular);
- The average friction angle is 36.6°, showing no significant correlation with the orientation of sedimentary bedding, nor with depth;
- A plateau in the shear force/displacement curve indicates the closing of a small gap between sample and shear box, which is not likely to affect results in a negative way;
- Moisture content makes an important contribution to the cohesion of Maastrichtian calcarenite, this could not be quantified in more detail however;
- Shear box tests yield unreliable and inconsistent results when they are not performed according to standards: the vertical position and alignment of the sample in the box is of great influence on the proper development of a continuous shear plane;
- UCS can be estimated from the cohesion and friction angle obtained by shear box tests. This gives fair, but not highly accurate approximations, since estimations deviate by up to ±25% from actual UCS.

8 Recommendations

After having been busy with testing and analysing the strength of calcarenite by different manners for several weeks, some recommendations for further research can be made.

Since a large portion of the shear box tests gave irrelevant results, I would recommend to perform some additional shear box tests, but at more normal stresses per material, e.g. four to five different normal stresses ranging from about 50 to 250 kPa. This would yield more data points per C-phi curve and thus a lower sensitivity to anomalies and outliers, which would improve the reliability of the final results. Meanwhile, it is important to keep the distinction with respect to the orientation of the sedimentary bedding.

Besides, it would be highly interesting trying to quantify the effects of moisture content on cohesion, mainly, but also on friction angle. It is expected that, due to lack of surface tension, testing material in a completely dry state will cause the cohesion to decrease dramatically. On the other hand, full saturation is expected to let the cohesion decrease as well.

Furthermore, triaxial tests would also be a considerable option for further research, since these approach in situ conditions (confining stress) more closely and boundary conditions are better defined than for shear box tests. Especially extensional triaxial tests (with constant vertical stress and increasing lateral stress) could be carried out to simulate conditions at passive failure in the building pit. Sample preparation for triaxial tests could turn out to be very difficult, though, because the material is extremely weak: taking cores by drilling would certainly pre-damage the material too much, so everything has to be done by hand, which is prone to damage as well.

However, from own experience, the most important recommendation might be to study the standards carefully and perform tests according to them: mainly taking care that for shear box tests, the sample is in the vertical middle of the shear box.

References

A2 Maastricht (2013), *Homepage A2 Maastricht*, www.a2maastricht.nl
Consulted on 19 October 2013.

Allersma, H.G.B. (2005), *Optical analysis of stress and strain in shear zones*, Powders & Grains 2005 (Int. Conference), Taylor & Francis Group, London, pp. 187-191.

Avenue2 (2013), *Samenvatting laboratoriumonderzoek t.b.v. observational method* (hand-out for visitors to construction site).

Berendsen, H.J.A. (2008), *De vorming van het land: Inleiding in de geologie en morfologie*, Van Gorcum & Comp. B.V., Assen, pp. 68-72.

British Standard (BS) 1377 Part 7 (1990), pp. 4-11, 29-30.

Douglas, K.J. (2002), *The shear strength of rock masses*, University of New South Wales, Australia (PhD thesis).

Felder, W.M. (1989), *Kalkstenen uit het Boven-Krijt en Onder-Tertiair van Zuid-Limburg*, Grondboor en Hamer Vol. 43 No. 5/6, pp. 145-155.

Goodman, R.E. (1989), *Introduction to Rock Mechanics*, John Wiley & Sons, New York; 2nd edition.

International Commission on Stratigraphy (2013), *International Chronostratigraphic Chart*, v.2013/01, www.stratigraphy.org/ICSchart/ChronostratChart2013-01.pdf
Consulted on 18 October 2013.

Kouwenberg, P. (2009), *3D subsurface modelling and geotechnical risk analysis for the tunnel construction of the A2-project Maastricht*, Delft University of Technology (MSc thesis).

Lavoie, D. (1988), *Geotechnical properties of sediments in a carbonate-slope environment*, Proceedings of the Ocean Drilling Program, Scientific Results Vol. 101, pp. 315-326.

Lavoie, D.L. and Bryant, W.R. (1993), *Permeability Characteristics of Continental Slope and Deep-Water Carbonates from a Microfabric Perspective*, Frontiers in Sedimentary Geology: Carbonate Microfabrics, pp. 117-128.

Maurenbrecher, P.M. and Verwaal, W. (2007), *Description of core and gravel samples and the determination of geotechnical parameters. Project A2 municipality of Maastricht*, Delft University of Technology (internal document; project code TA/IG/07.016).

Ngan-Tillard, D.J.M et al. (2011), *Application of the needle penetration test to a calcarenite, Maastricht, the Netherlands*, Engineering Geology Vol. 123, pp. 214-224.

Oliveira, D.V., Lourenço, P.B. and Poca, P. (2006), *Cyclic behaviour of stone and brick masonry under uniaxial compressive loading*, Materials and Structures Vol. 39 No. 2, pp. 247-257.

Sandoval, E.A. and Pando, M.A. (2012), *Experimental assessment of the liquefaction resistance of calcareous biogenous sands*, Earth Sciences Research Journal Vol. 16 No. 1, pp. 55-63.

Servais, R. (2013), Strukton, *Site investigation and application of the observational method on the A2 tunnel Maastricht* (?) (guest lecture / PowerPoint presentation).

Shibuya, S., Mitachi, T., and Tamate, S. (1997), *Interpretation of direct shear box testing of sands as quasi-simple shear*, Géotechnique Vol. 47 No. 4, pp. 769-790.

Van Dalen, J. (2011), Strukton, *Soil investigation Tunnel A2 Maastricht* (guest lecture / PowerPoint presentation).

Wesselingh, F. et al. (2011), Naturalis, *Reconstructies Tijdvakken: Krijt & Paleoceen*, www.geologievannederland.nl/tijd/reconstructies-tijdvakken
Consulted on 18 October 2013.

Appendix A (part 1 of 2)

Overview map of the A2 tunnel construction site

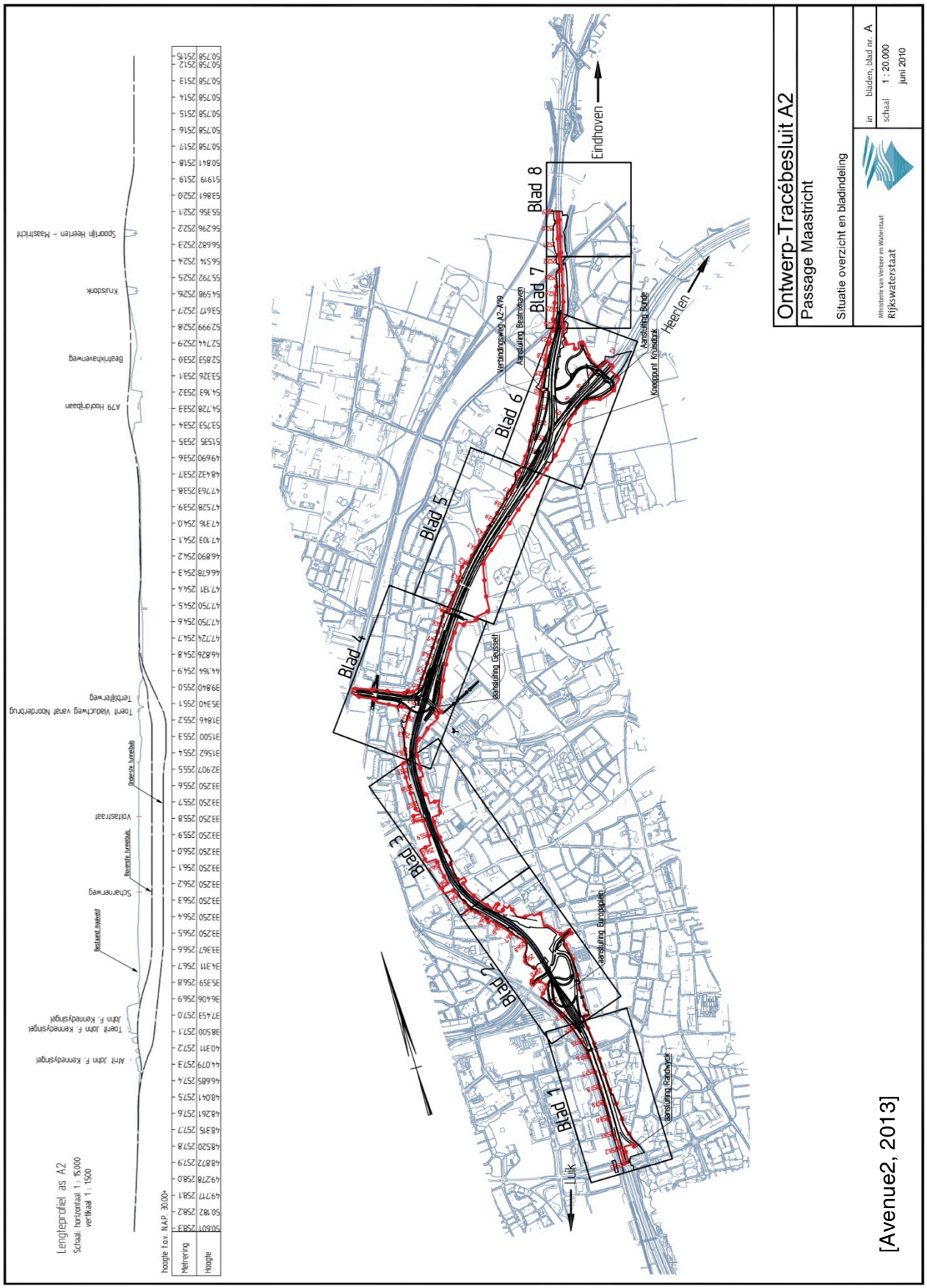

Appendix A (part 2 of 2)

Overview map of the A2 tunnel construction site: Geusselt section

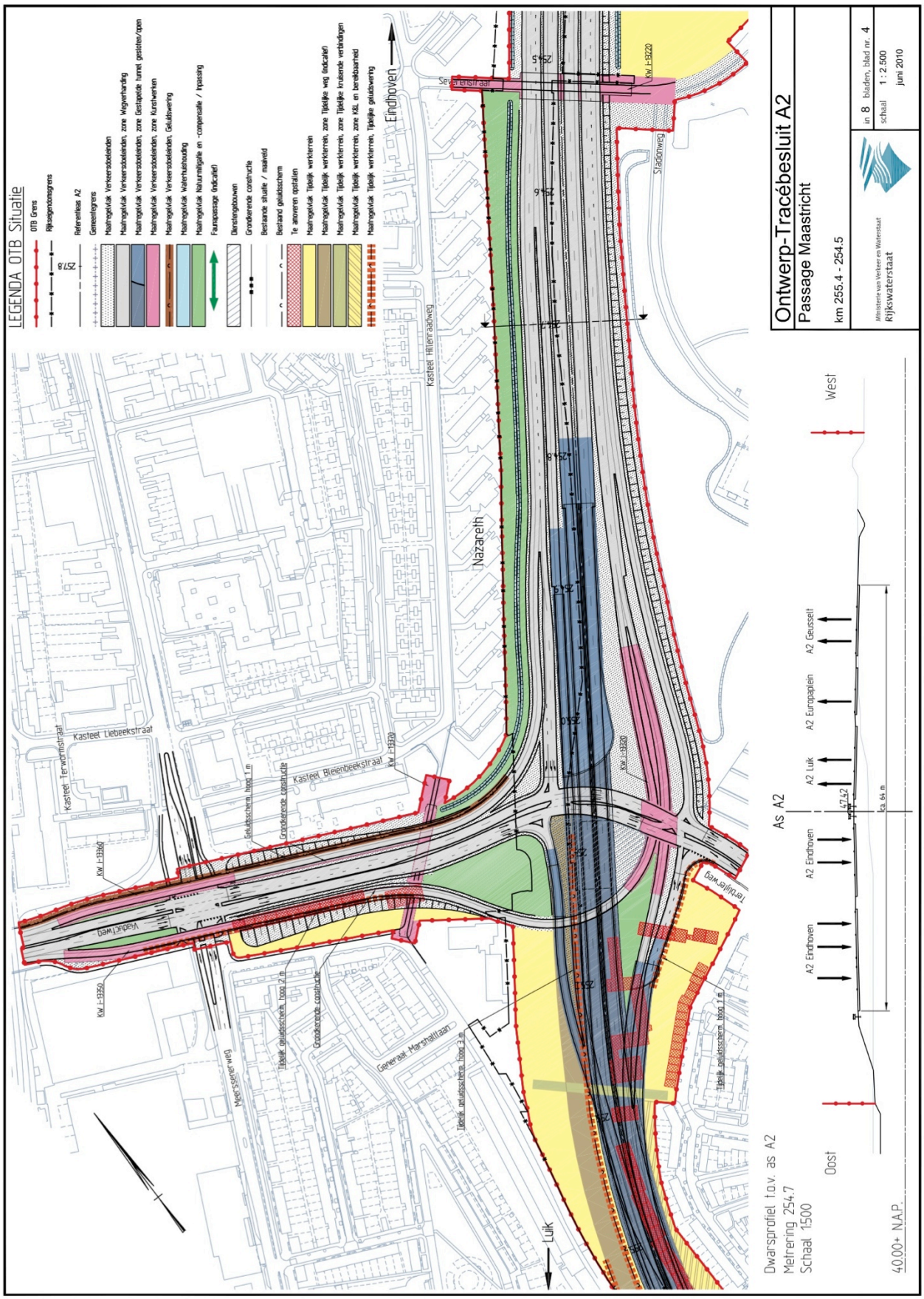

[Avenue2, 2013]

Appendix B (part 1 of 5)

Previously obtained results: borehole situation

Sampling location

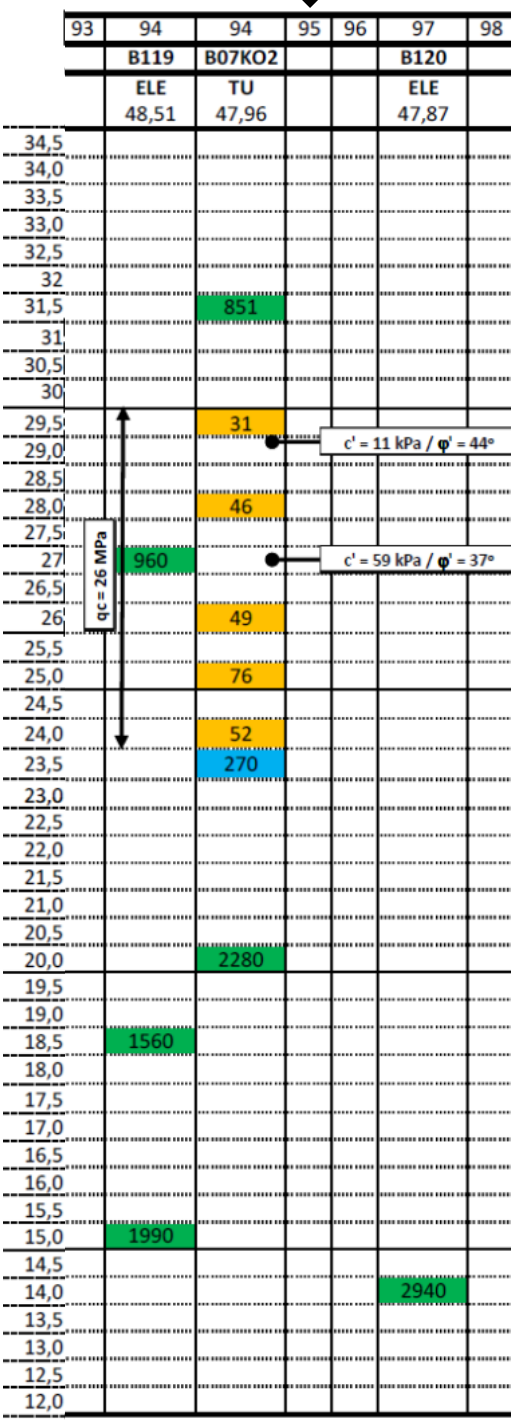

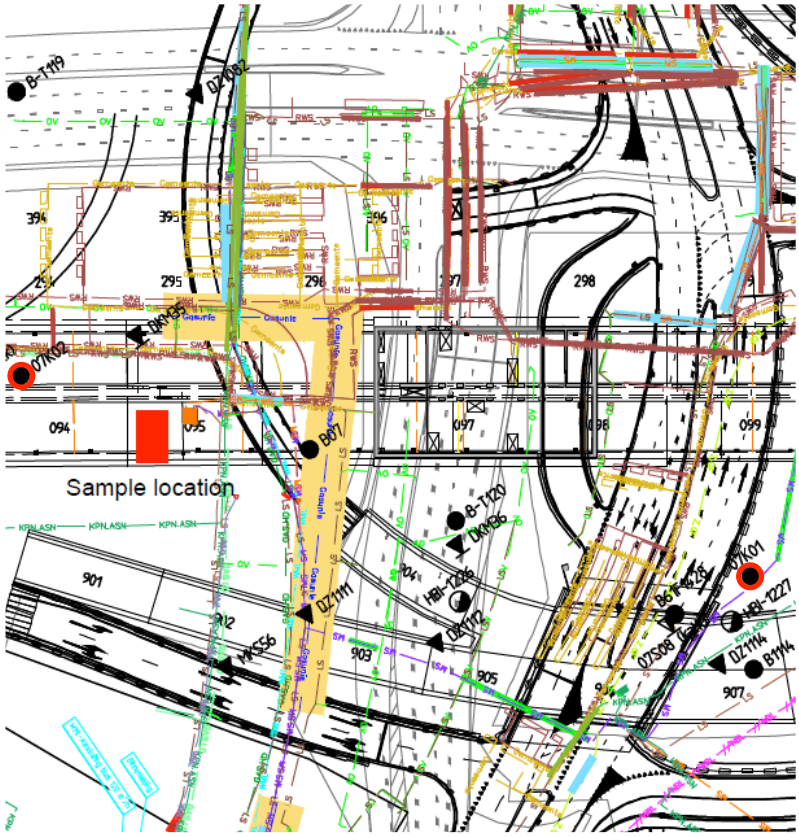

Detail map of the sampling location (red square) in the Geusselt section of the A2 tunnel. The most nearby boreholes (B07k02 and B07k01) are also marked (encircled) red.

[Avenue2, 2013]

Appendix B (part 2 of 5)

Previously obtained results from triaxial and shear box tests

Results

Sample	Angle of friction	Cohesion kPa
B07k02 18.50m 18.6m 18.70m	43.9	11.0
B07k02 20.60m 20.70m 20.85m	37.1	59.2
B07k03 16.10m 16.20m 16.30m	35.8	43.2
B07k03 19.30m 19.40m 19.50m	42.2	15.3
B07k04 15.10m 15.20m 15.30m	44.8	8.8
B07k04 15.50m 15.60m 16.70m	40.7	41.2
B07k04 18.50m 18.60m 18.70m	42.5	7.5
B07k05 19.80m 20.10m 20.85m	35.8	172.8
B07k07 17.10m 17.20m	21.6	1208

One direct shear box test was performed on the softened material from a supplied container of B07k05 15.70m-17.20m. The direct shear box used has a diameter of 62.5mm and a shear speed of 1mm/min. The stress-strain graph and a graph of normal stress against shear stress are given at the end of this section

Results

sample	Angle of friction	Cohesion kPa
B07k05 15.70m-17.20m	36.8	0

B07k05 15-70-17.20 shear box test normal stress - shear stress, angle of friction is 36.8 cohesion 0 kPa

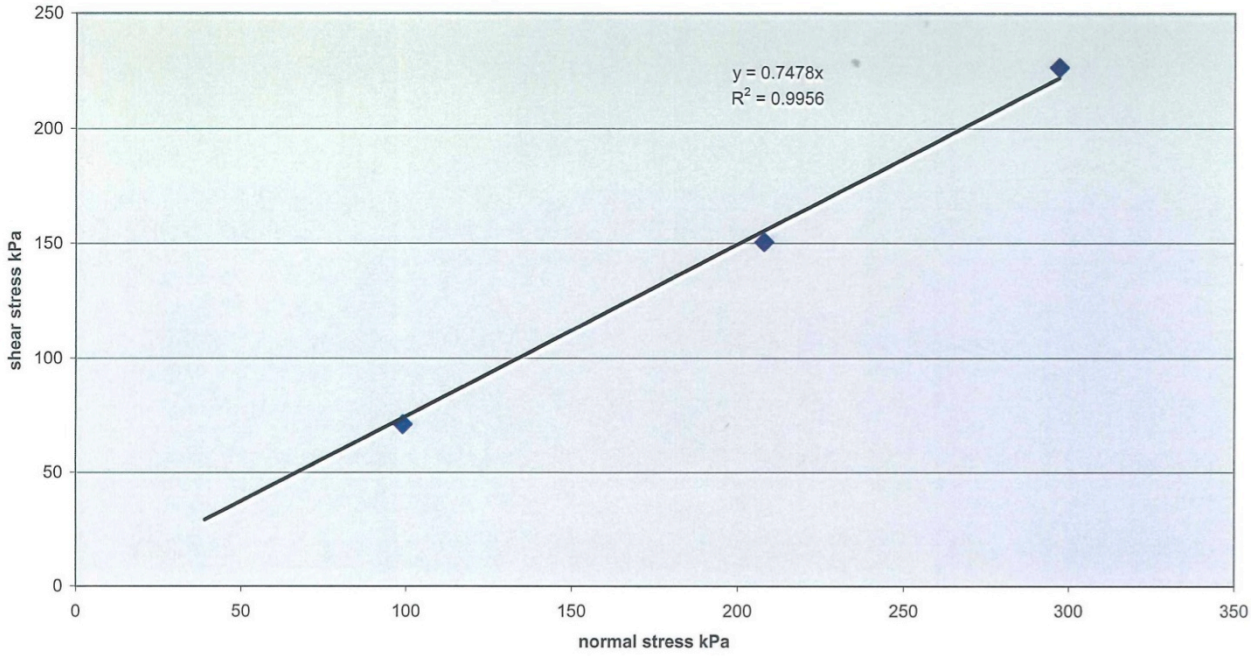

[Maurenbrecher & Verwaal, 2007]

Appendix B (part 3 of 5)

Previously obtained results from UCS tests

ucs tests

	sample			*			sample for determination water content			remarks	bulk density	water	dry mass	dry		E-mod. At
core	number	depth	diameter	length	mass	max load	massa wet	massa dry	massa cup		during testing	content	during testing	density	ucs	50% ucs
		m	mm	mm	g	N	g	g	9.00		mg/m^3	%	g	mg/m^3	kPa	MPa
													g			
b07k01	ucs 48	13.95	49.2	100.1	337.96						1.78	40.16	241.13	1.27	560.0	100.0
b07k01	ucs 54	15.50	49.2	80.5	271.76						1.78	39.77	194.43	1.27	820.0	170.0
b07k01	ucs 37	18.60	49.7	96.1	346.17	74	408.04	339.09	94.11		1.86	28.15	270.14	1.45	38.1	4.4
b07k01	ucs 52	22.20	49.2	96.8	341.79						1.86	33.36	256.29	1.39	1550.0	460.0
b07k01	ucs 38	24.10	50.0	95.8	346.50	95	475.89	388.96	93.97		1.84	29.47	267.63	1.42	48.4	2.9
b07k02	ucs 10	16.40	54.5	101.5	422.21	1984	380.26	303.10	94.44		1.78	36.98	308.23	1.30	850.9	178.0
b07k02	ucs 13	18.00	49.8	96.5	330.53	61	654.60	525.70	140.60		1.76	33.47	247.64	1.32	31.3	2.5
b07k02	ucs 14	19.85	50.0	109.0	391.32	91	480.79	401.38	93.55		1.83	25.80	311.07	1.45	46.4	4.4
b07k02	ucs 11	21.50	53.5	103.0	428.88	109	480.97	399.60	94.94		1.85	26.71	338.48	1.46	48.5	4.2
b07k02	ucs 15	22.80	50.0	106.0	367.64	149	456.73	368.10	93.94		1.77	32.33	277.83	1.34	75.9	7.2
b07k02	ucs 16	24.00	50.0	101.9	358.71	102	508.10	403.91	93.67		1.79	33.58	268.53	1.34	52.0	5.7
b07k02	ucs 17	24.25	50.0	101.7	360.02	529	417.20	331.64	96.73		1.80	36.42	263.90	1.32	269.6	30.0
b07k02	ucs 27	27.80	49.3	90.0	313.89						1.83	37.86	227.68	1.33	2280.0	640.0
b07k03	ucs 53	13.55	49.2	90.5	308.27						1.79	39.19	221.47	1.29	970.0	250.0
b07k03	ucs 40	15.10	49.4	72.3	245.84	102	539.21	422.83	94.75		1.78	35.47	181.47	1.31	53.3	6.5
b07k03	ucs 41	17.70	50.0	92.0	317.84	111	495.64	393.38	94.72		1.76	34.24	236.77	1.31	56.6	4.0
b07k03	ucs 42	17.95	49.8	83.6	294.25	217	502.24	410.82	93.71		1.81	28.83	228.40	1.40	111.4	11.2
b07k03	ucs 47	21.30	49.2	97.1	323.54						1.75	45.03	223.09	1.21	1480.0	400.0
b07k03	ucs 43	22.70	49.5	92.5	313.82		335.12	269.90	94.72		1.76	37.23	228.68	1.29	44.7	5.1

[Maurenbrecher & Verwaal, 2007]

Appendix B (part 4 of 5)

Previously obtained results from UCS tests

ucs tests

	sample						sample for determination water content			remark	bulk density	water	dry mass	dry		E-mod. At
core	number	depth	diameter	length	mass	max load	massa wet	massa dry	massa cup		during testing	content	during testing	density	ucs	50% ucs
		m	mm	mm	g	N	g	g	9.00		mg/m³	%	g	mg/m³	kPa	MPa
b07k03	ucs 45	23.55	52.0	98.5	394.25	91	489.86	393.25	94.25		1.89	32.31	297.97	1.43	42.9	3.2
b07k03		24.35								mislukt						
b07k03	ucs 44	25.20	50.4	78.5	280.01	1975	452.68	352.99	93.66		1.79	38.44	202.26	1.29	990.5	117.9
b07k04	ucs 1	15.80	49.1	101.7	347.09	859	456.92	379.02	140.56		1.80	32.67	261.62	1.36	453.9	67.0
b07k04	ucs 2	16.25	50.0	101.7	369.98	95	480.04	405.71	138.90		1.85	27.86	289.37	1.45	48.4	3.7
b07k04	ucs 3	17.13	50.6	97.0	355.79	375	511.56	429.22	140.22		1.82	28.49	276.90	1.42	186.6	20.8
b07k04	ucs 4	17.24	50.5	102.5	371.92	120	364.43	302.52	94.11		1.81	29.71	286.74	1.40	59.9	5.6
b07k04	ucs 5	17.55	51.0	101.7	395.66	106	382.15	316.71	93.90		1.91	29.37	305.84	1.47	51.9	4.3
b07k04	ucs 6	18.40	50.0	101.7	377.44	90	428.53	354.63	93.98		1.89	28.35	294.07	1.47	45.9	2.2
b07k04	ucs 7	20.60	50.1	101.7	361.42	70	383.13	312.91	96.67		1.80	32.47	272.83	1.36	35.5	3.8
b07k04	ucs 9	26.15	53.4	88.4	361.51		390.22	317.49	94.13		1.83	32.56	272.71	1.38	1540.0	660.0
b07k04	ucs 26	26.75	49.3	100.5	363.43						1.90	33.17	272.91	1.42	2320.0	760.0
b07k04	ucs 29	27.95	49.5	84.8	307.13						1.88	31.83	232.97	1.43	1210.0	250.0
b07k04	ucs 25	30.10	49.9	104.0	377.73						1.86	32.86	284.30	1.40	2280.0	520.0
b07k05	ucs 39	18.80	49.9	99.1	326.58	65	347.24	297.55	94.14		1.69	24.43	262.46	1.35	33.3	2.2
b07k05	ucs 12	19.25	50.5	88.5	322.84	2170	435.19	349.94	94.12		1.82	33.32	242.15	1.37	1083.9	262.4
b07k05	ucs 33 2e load	20.70	51.5	74.4	279.00						1.83	37.20	203.36	1.31	1200.0	310.0
b07k05	ucs 34	23.50	48.5	97.4	338.59	723	460.00	370.36	96.60		1.88	32.74	255.07	1.42	391.5	47.6
b07k05	ucs 35	25.50	52.4	85.2	322.67	595	466.89	382.77	93.93		1.76	29.12	249.89	1.36	276.0	31.9
b07k05	ucs 36	28.50	50.30	99.34	360.10	1062	491.06	396.87	93.88		1.83	31.09	274.70	1.39	534.7	58.1

[Maurenbrecher & Verwaal, 2007]

Appendix B (part 5 of 5)

Previously obtained results from UCS tests

ucs tests

	sample						sample for determination water content			remar	bulk density	water	dry mass	dry		E-mod. At
core	number	depth	diameter	length	mass	max load	massa wet	massa dry	massa cup		during testing	content	during testing	density	ucs	50% ucs
		m	mm	mm	g	N	g	g	9.00		mg/m^3	%	g	mg/m^3	kPa	MPa
b07k05	ucs 49	29.90	49.6	100.3	374.40						1.93	29.78	288.48	1.49	2290.0	660.0
b07k05	ucs 51	30.70	49.7	100.2	384.62						1.98	26.01	305.24	1.57	4350.0	1460.0
b07k06	ucs 24	17.00	49.2	89.0	307.99						1.82	36.54	225.57	1.33	1150.0	320.0
b07k06	ucs 23	18.10	48.5	94.5	324.51						1.86	35.64	239.24	1.37	1360.0	440.0
b07k06	ucs 21	21.80	49.4	103.4	386.99						1.95	28.13	302.03	1.52	2590.0	790.0
b07k06	ucs 22	25.50	49.6	84.4	327.70						2.01	25.28	261.58	1.60	2860.0	690.0
b07k06	ucs 55	25.70	49.0	83.6	312.44						1.98	26.71	246.57	1.56	1730.0	750.0
b07k07	ucs 20	18.80	49.5	96.3	362.67						1.96	27.83	283.72	1.53	2380.0	810.0
b07k07	ucs 18	24.30	49.5	98.2	374.05						1.98	26.06	296.73	1.57	3740.0	1570.0
b07k07	ucs 19	30.10	49.8	104.7	428.63						2.10	18.33	362.22	1.78	4940.0	1560.0
b07k08	ucs 50	18.90	49.6	100.6	368.75						1.90	30.44	282.70	1.46	1730.0	630.0
b07k08	ucs 46	21.35	49.5	100.0	367.17						1.91	30.76	280.79	1.46	1660.0	640.0
b07k09	ucs 28	17.70	49.5	85.8	312.11						1.89	31.97	236.50	1.43	1620.0	370.0
b07k09	ucs 30	17.90	49.7	101.2	416.81						2.12	18.95	350.40	1.79	7720.0	3770.0
b07k09	ucs 31	21.00	49.6	100.8	388.78						2.00	25.87	308.87	1.59	3080.0	1100.0
b07k09	ucs 32	22.50	49.5	103.4	398.06						2.00	25.77	316.50	1.59	2980.0	840.0

[Maurenbrecher & Verwaal, 2007]

Appendix C (part 1 of 4)

Shear box test graphs

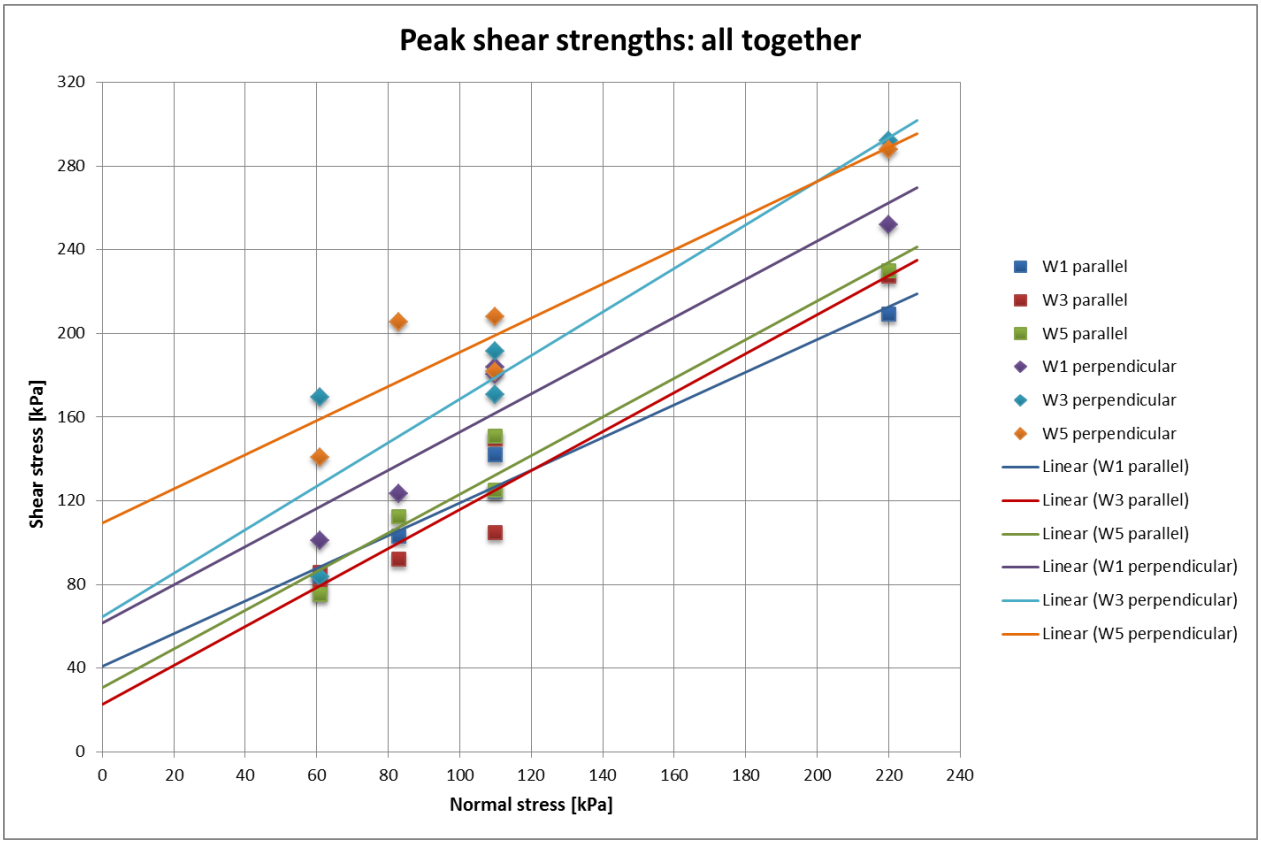

Figure C.1: Shear strength vs. normal stress (C-phi diagram) for all tests together, with linear trend lines.

Table C.1: Cohesions, friction angles and estimated UCS (Mohr-Coulomb) for all tests together.

	Cohesion [kPa]		**Friction angle [°]**		**UCS [kPa]**	
	parallel	perpendicular	parallel	perpendicular	parallel	perpendicular
W1	40,85	61,26	37,99	42,43	167,5	278,0
W3	22,70	64,59	42,96	46,15	104,3	320,9
W5	30,63	109,24	42,78	39,28	140,1	460,9

Appendix C (part 2 of 4)

Shear box test graphs

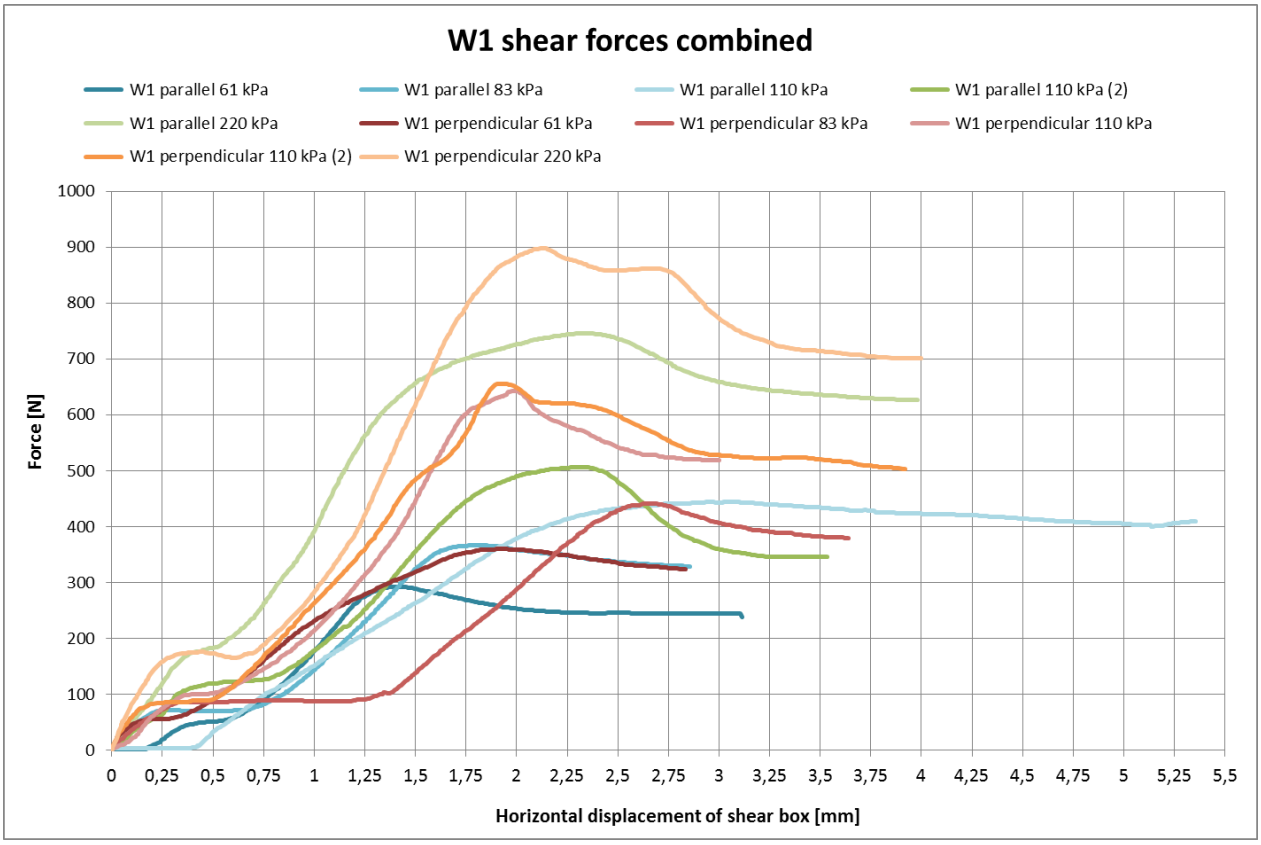

Figure C.2: Shear force vs. horizontal displacement for all shear box tests on W1.

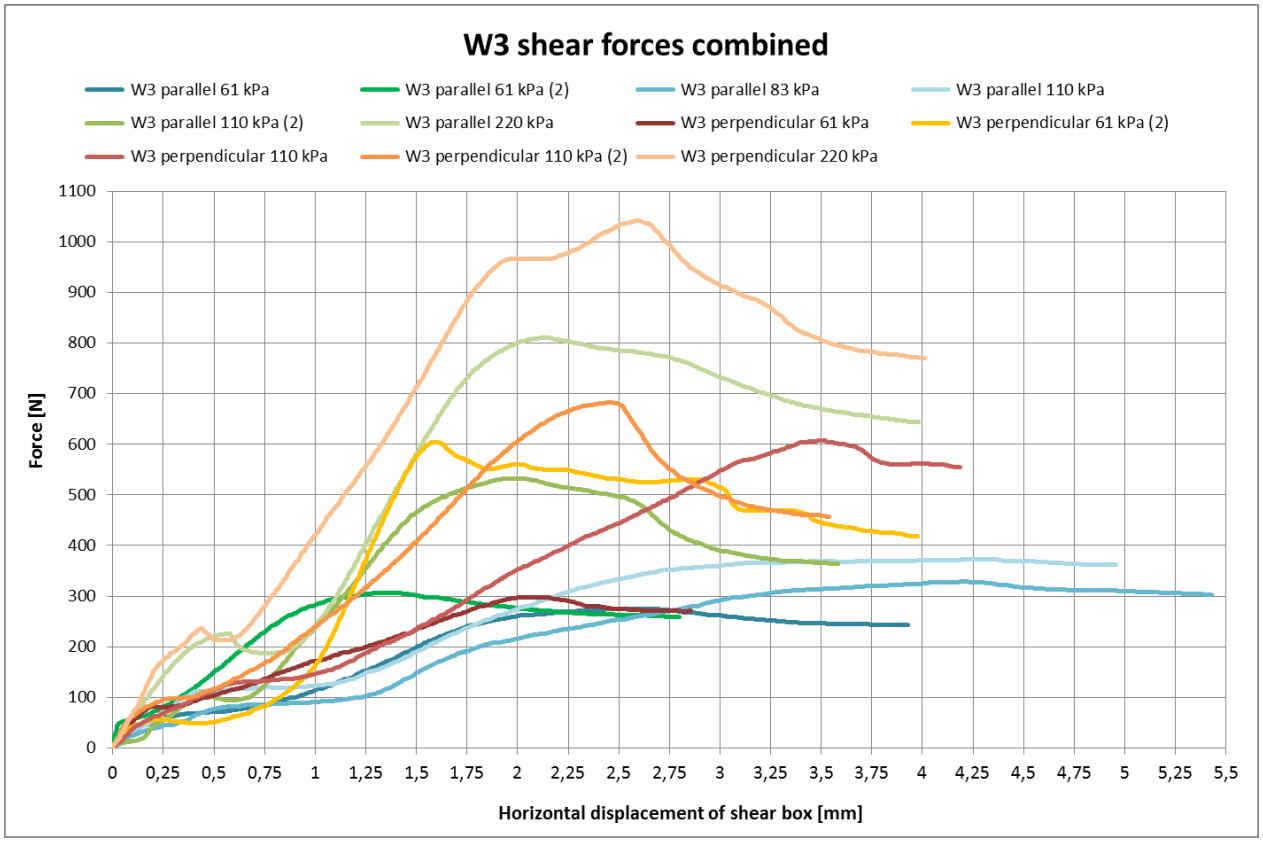

Figure C.3: Shear force vs. horizontal displacement for all shear box tests on W3.

Appendix C (part 3 of 4)

Shear box test graphs

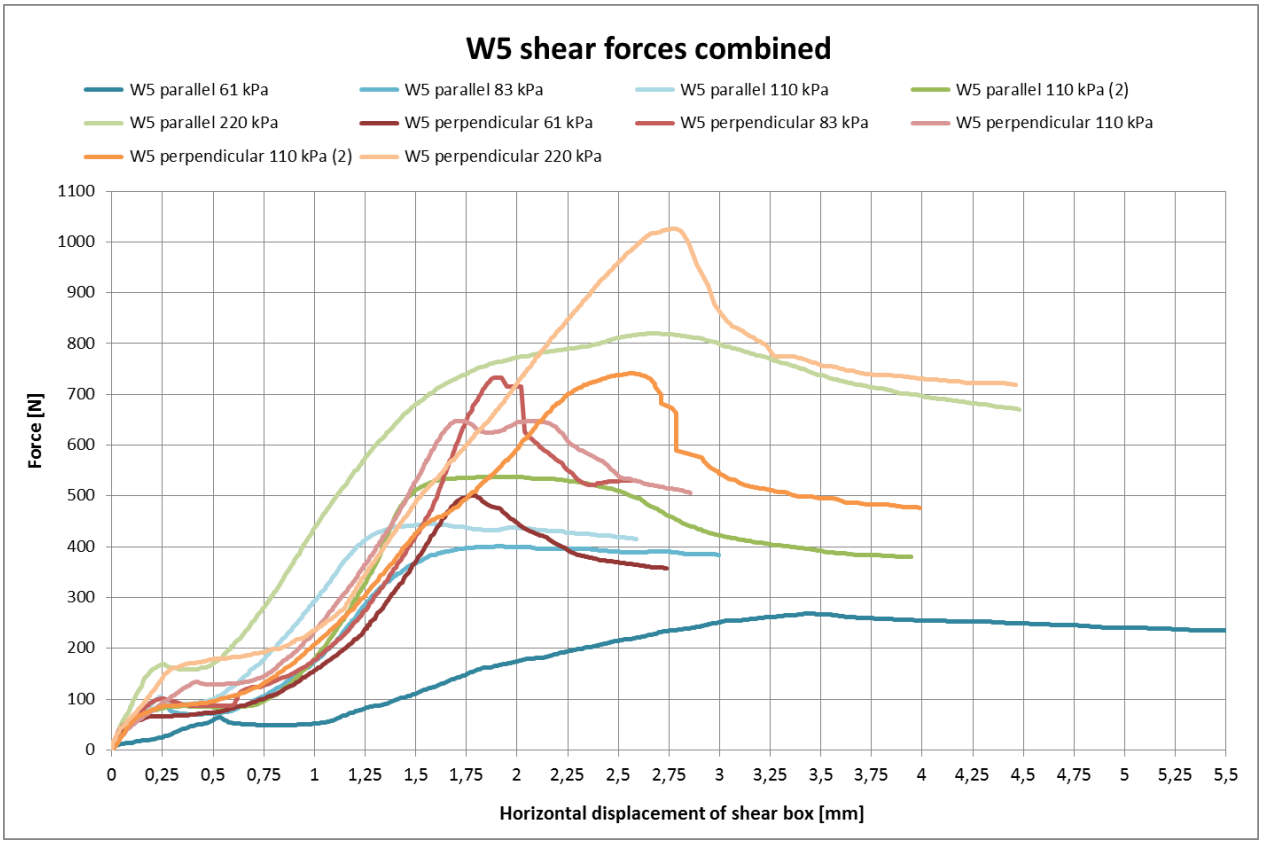

Figure C.4: Shear force vs. horizontal displacement for all shear box tests on W5.

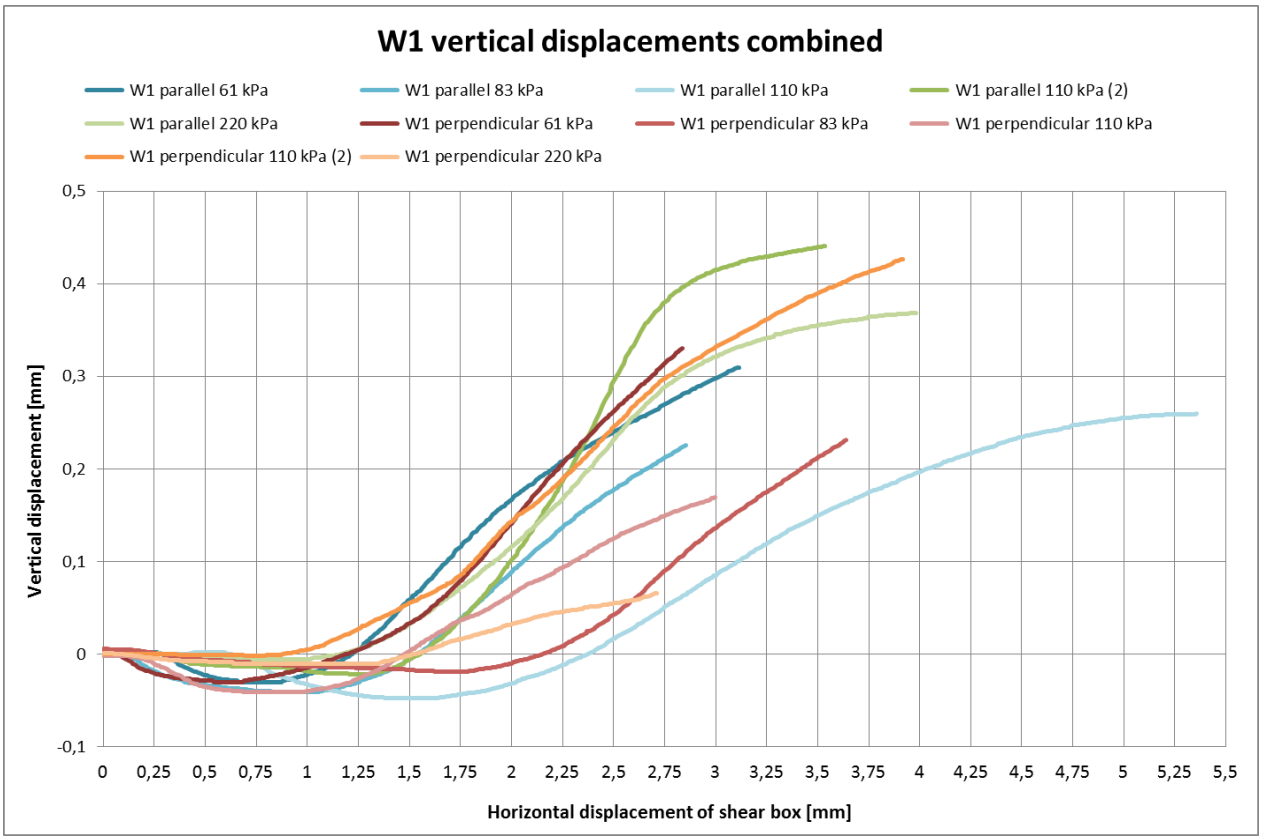

Figure C.5: Vertical displacement (dilation) during shear box tests on W1.

Appendix C (part 4 of 4)

Shear box test graphs

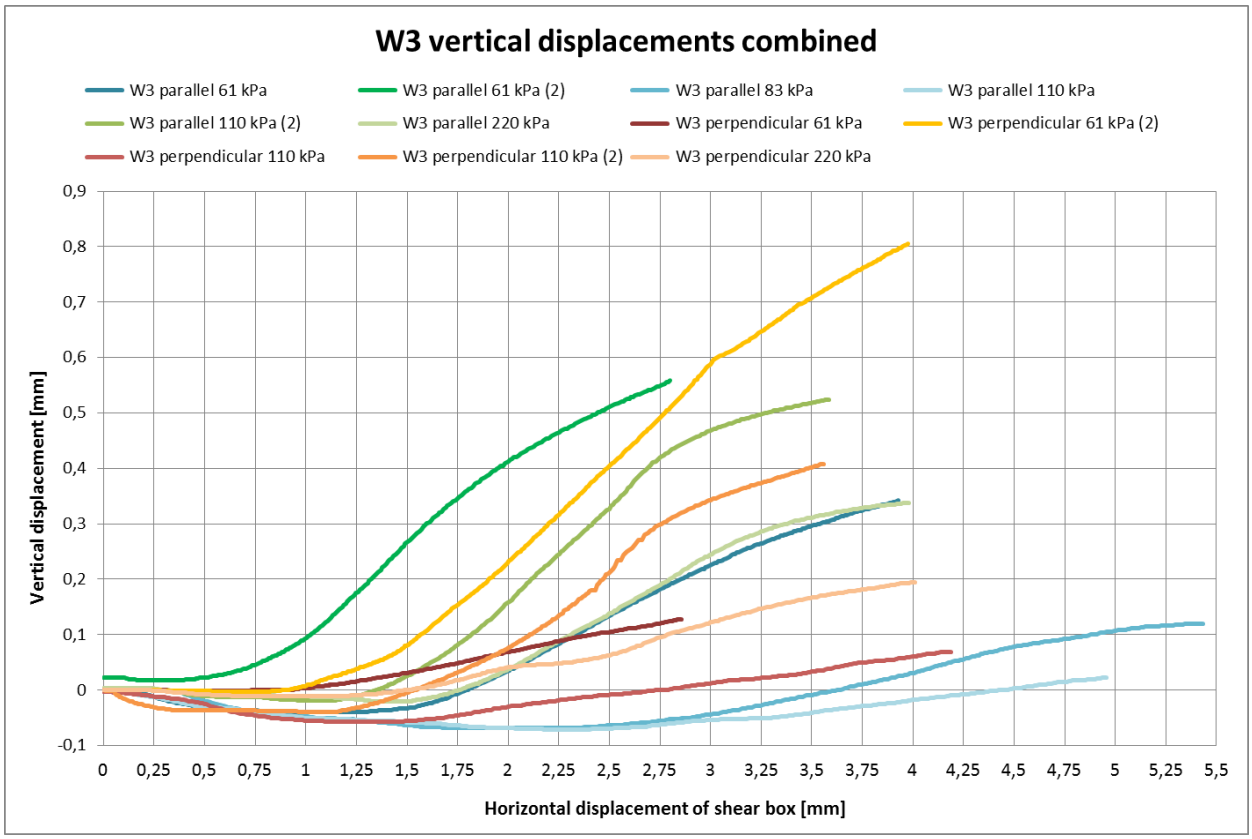

Figure C.6: Vertical displacement (dilation) during shear box tests on W3.

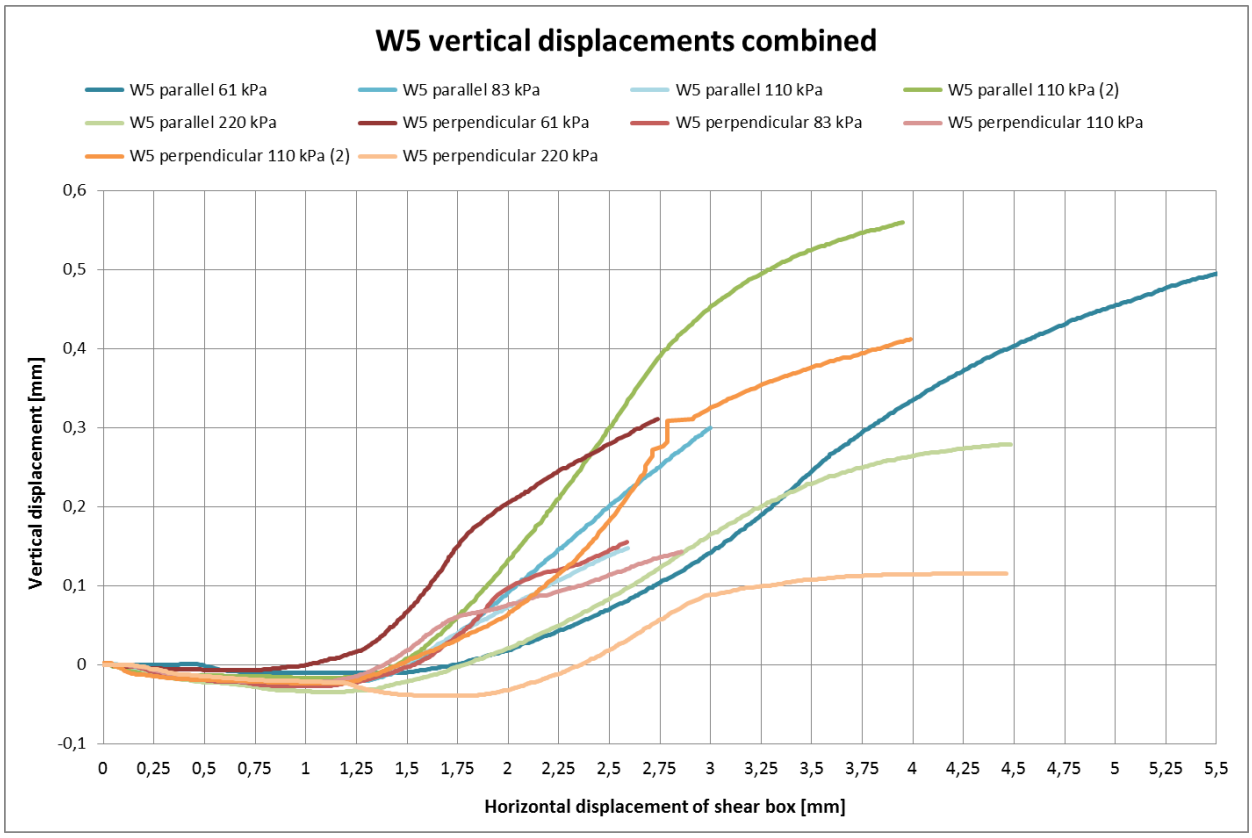

Figure C.7: Vertical displacement (dilation) during shear box tests on W5.

Appendix D

Shear box test results with subtraction of sliding friction

Table D.1: Measured shear strengths, corrected for sliding friction (all units in kPa). The first series of tests is marked by a light grey colour.

	Normal stress	parallel	perpendicular
W1	61	67,6	85,5
	83	83,3	98,9
	110	122,2	152,2
	110 (2)	107,4	159,8
	220	158,5	205,9
W3	61	56,9	61,3
	61 (2)	71,6	155,8
	83	68,0	
	110	71,2	133,9
	110 (2)	123,1	164,3
	220	175,0	232,3
W5	61	61,8	122,2
	83	92,7	181,3
	110	99,4	145,5
	110 (2)	127,6	183,1
	220	185,8	236,4

Table D.2: Cohesions, friction angles and estimated UCS (Mohr-Coulomb) for the first series of tests at normal stresses of 61, 83 and 110 kPa (corrected for sliding friction).

	Cohesion [kPa]		Friction angle [°]		UCS [kPa]	
	parallel	perpendicular	parallel	perpendicular	parallel	perpendicular
W1	0	0	47,1	53,0	0	0
W3	41,2	0	16,0	49,4	109,1	0
W5	21,3	115,1	36,8	22,2	85,0	342,6

Table D.3: Cohesions, friction angles and estimated UCS (Mohr-Coulomb) for the second series of tests at normal stresses of 61 kPa (2), 110 kPa (2) and 220 kPa (corrected for sliding friction).

	Cohesion [kPa]		Friction angle [°]		UCS [kPa]	
	parallel	perpendicular	parallel	perpendicular	parallel	perpendicular
W1	56,4	113,7	24,9	22,4	176,7	339,9
W3	42,4	118,4	31,8	26,8	152,4	384,6
W5	69,4	129,8	27,9	25,8	230,4	414,2

Table D.4: Cohesions, friction angles and estimated UCS (Mohr-Coulomb) for all tests together (corrected for sliding friction).

	Cohesion [kPa]		Friction angle [°]		UCS [kPa]	
	parallel	perpendicular	parallel	perpendicular	parallel	perpendicular
W1	43,9	54,7	28,7	36,3	148,1	216,1
W3	17,7	62,1	35,5	37,9	68,7	253,9
W5	27,4	102,0	36,4	31,6	108,4	364,5

Appendix E (part 1 of 2)

Moisture content of shear box tested samples

Material [1]	cup #	m_{cup}	m_{moist}	m_{dry}		Moist. content [2]		Moist. content [3]	
W1.1 61+83+110 (1)	SF	94,60	209,65	199,84	g	9,32	%	8,53	%
W1.1 110 (2) + 220	SF	94,60	193,93	184,24	g	10,81	%	9,76	%
W1.2 61	SG	96,65	327,07	305,51	g	10,32	%	9,36	%
W1.2 83	RJ#8	93,93	207,01	196,23	g	10,54	%	9,53	%
W1.2 110 (2) + 220	A3	93,99	231,70	218,15	g	10,91	%	9,84	%
W3b.1	A3	93,99	277,00	254,98	g	13,68	%	12,03	%
W3b.2	SF	94,60	170,92	160,29	g	16,18	%	13,93	%
W3a.1 61 (2)	A2	94,44	304,14	281,41	g	12,16	%	10,84	%
W3a.1 110 (2) + 220	A2	94,44	273,18	251,64	g	13,70	%	12,05	%
W3a.2 61 (2)	A1	93,53	365,93	328,73	g	15,82	%	13,66	%
W3a.2 110 (2) + 220	SG	96,65	306,51	277,73	g	15,89	%	13,71	%
W5.1 61+83+110 (1)	SG	96,65	277,50	256,97	g	12,81	%	11,35	%
W5.1 110 (2) + 220	SG	96,65	199,12	187,64	g	12,62	%	11,20	%
W5.2 61+110 (1)	A3	93,99	204,09	190,60	g	13,96	%	12,25	%
W5.2 83	A3	93,99	244,40	225,24	g	14,60	%	12,74	%
W5.2 110 (2)	RJ#8	93,93	218,58	203,60	g	13,66	%	12,02	%
W5.2 220	A3	93,99	271,05	249,79	g	13,65	%	12,01	%

Remarks

(1) Terminology: x.1 = parallel, x.2 = perpendicular.
(2) Moisture content with respect to dry mass, according to BS 1377:7 (1990) section 4.6.1.1.
(3) Moisture content with respect to moist mass.

Appendix E (part 2 of 2)

Saturation of shear box tested samples

Material	m_{moist} (1)		bulk density		V_{water} (2)	V_{solids} (3)	V_{void}	void ratio	Saturation
W1.1 61	259,60	g	1,30	g/cm³	7,89	31,11	39,82	1,28	0,20
W1.1 83	N/A								
W1.1 110	1257,70	g (4)	1,33	g/cm³	8,02	31,65	39,28	1,24	0,20
W1.1 110 (2)	262,32	g	1,34	g/cm³	9,29	31,59	39,33	1,25	0,24
W1.1 220	262,20	g	1,34	g/cm³	9,28	31,55	39,37	1,25	0,24
W1.2 61	261,53	g	1,33	g/cm³	8,84	31,47	39,46	1,25	0,22
W1.2 83	261,42	g	1,33	g/cm³	8,99	31,37	39,55	1,26	0,23
W1.2 110	262,16	g	1,34	g/cm³	8,89	31,68	39,25	1,24	0,23
W1.2 110 (2)	263,55	g	1,36	g/cm³	9,49	31,97	38,95	1,22	0,24
W1.2 220	262,52	g	1,35	g/cm³	9,39	31,63	39,30	1,24	0,24
W3b.1 61	259,46	g	1,30	g/cm³	11,11	29,87	41,05	1,37	0,27
W3a.1 61 (2)	266,45	g	1,40	g/cm³	10,77	32,57	38,36	1,18	0,28
W3b.1 83	262,50	g	1,35	g/cm³	11,48	30,85	40,07	1,30	0,29
W3b.1 110	260,36	g	1,31	g/cm³	11,22	30,16	40,76	1,35	0,28
W3a.1 110 (2)	267,65	g	1,42	g/cm³	12,12	32,51	38,41	1,18	0,32
W3a.1 220	269,13	g	1,44	g/cm³	12,30	32,99	37,93	1,15	0,32
W3b.2 61	274,75	g	1,52	g/cm³	14,99	34,06	36,86	1,08	0,41
W3a.2 61 (2)	274,99	g	1,52	g/cm³	14,73	34,25	36,68	1,07	0,40
W3b.2 110	272,47	g	1,49	g/cm³	14,68	33,34	37,58	1,13	0,39
W3a.2 110 (2)	267,68	g	1,42	g/cm³	13,79	31,91	39,02	1,22	0,35
W3a.2 220	274,07	g	1,51	g/cm³	14,67	33,93	36,99	1,09	0,40
W5.1 61	267,11	g	1,41	g/cm³	11,35	32,59	38,33	1,18	0,30
W5.1 83	264,40	g	1,37	g/cm³	11,05	31,71	39,21	1,24	0,28
W5.1 110	272,80	g	1,49	g/cm³	12,00	34,45	36,48	1,06	0,33
W5.1 110 (2)	267,73	g	1,42	g/cm³	11,27	32,85	38,07	1,16	0,30
W5.1 220	265,63	g	1,39	g/cm³	11,04	32,17	38,76	1,20	0,28
W5.2 61	272,40	g	1,48	g/cm³	12,90	33,97	36,96	1,09	0,35
W5.2 83	272,38	g	1,48	g/cm³	13,41	33,78	37,15	1,10	0,36
W5.2 110	273,13	g	1,49	g/cm³	12,99	34,21	36,72	1,07	0,35
W5.2 110 (2)	274,23	g	1,51	g/cm³	12,87	34,65	36,27	1,05	0,35
W5.2 220	271,58	g	1,47	g/cm³	12,55	33,80	37,13	1,10	0,34

Remarks

(1) Bulk mass in cutting mould (m_{mould} = 167.1 g, V_{mould} = 70.9 cm^3).
(2) Based on moisture content with respect to *moist mass*.
(3) Specific gravity of Maastrichtian calcium carbonate = 2.72 g/cm^3, obtained by measurement with a helium pycnometer [Ngan-Tillard et al., 2011].
(4) Weighed in shear box ($m_{shearbox}$ = 1163.6 g, V = V_{mould})

Appendix F (part 1 of 3)

Selection of photographs from visit to construction site

Appendix F (part 2 of 3)

Selection of photographs from visit to construction site

Appendix F (part 3 of 3)

Selection of photographs from visit to construction site

Appendix G (part 1 of 3)

Selection of photographs from laboratory work

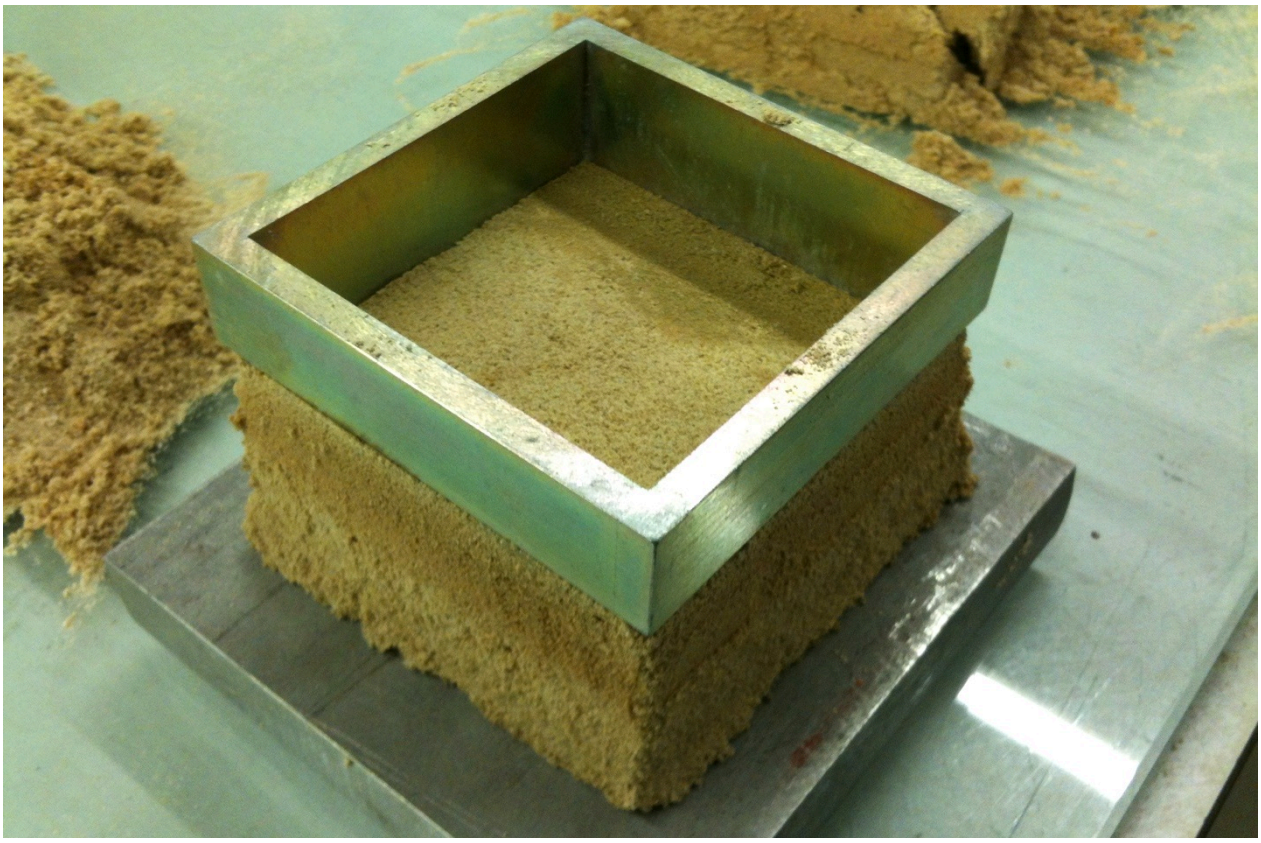

Appendix G (part 2 of 3)

Selection of photographs from laboratory work

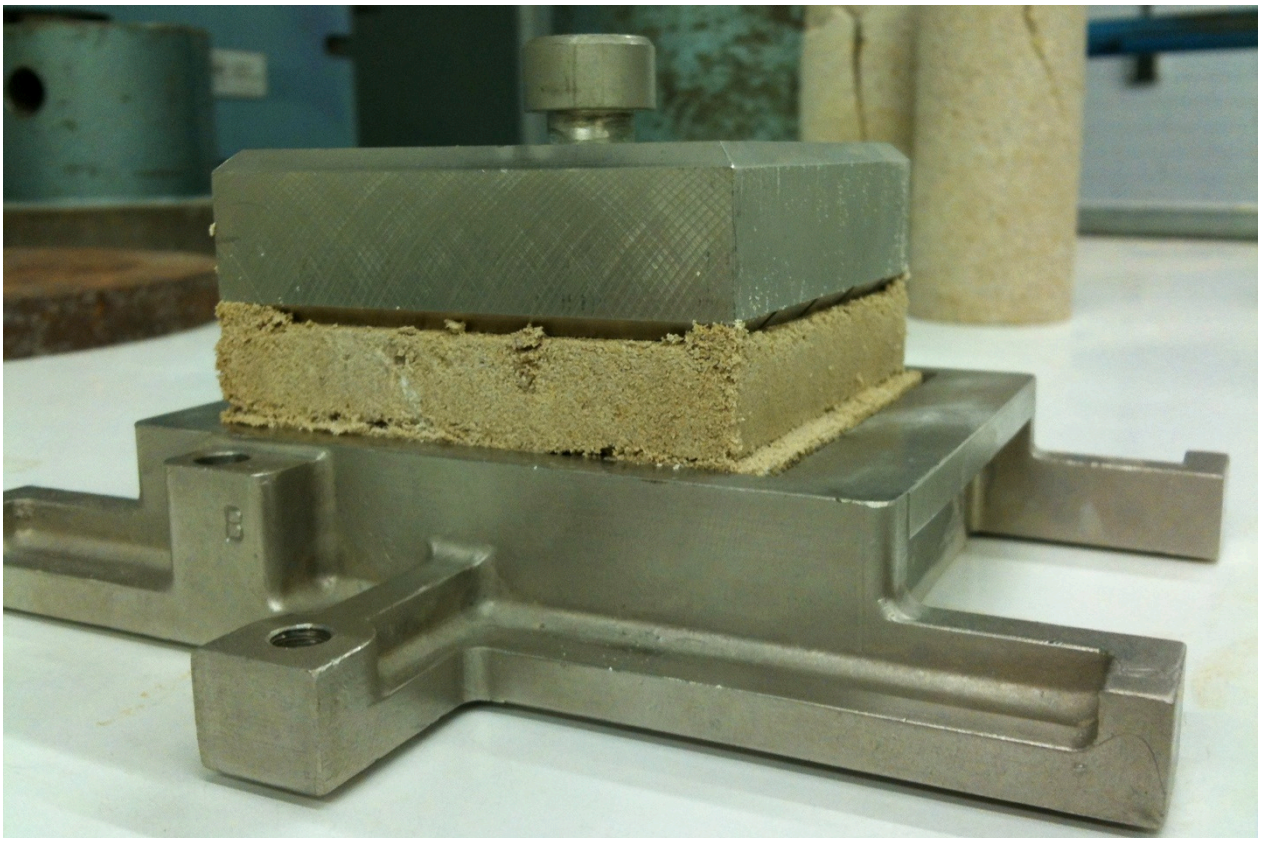

Appendix G (part 3 of 3)

Selection of photographs from laboratory work